International Journal of Communication Systems

WILEY

RESEARCH ARTICLE

PAPR Reduction Using Discrete Forest Optimization Algorithm Based on SLM Technique in Intensity Modulated Direct Detection Optical OFDM Communication Systems

Mahmoud Alhalabi[1] | Necmi Taşpınar[2] | Mohammed Wadi[1]

[1]Department of Electrical and Electronics Engineering, Istanbul Sabahattin Zaim University, Istanbul, Turkey | [2]Department of Electrical and Electronics Engineering, Erciyes University, Kayseri, Turkey

Correspondence: Mahmoud Alhalabi (mahmoud.alhalabi@izu.edu.tr)

Received: 20 January 2025 | **Revised:** 1 May 2025 | **Accepted:** 6 May 2025

Funding: This research was supported by the Erciyes University Scientific Research Projects Coordination Unit (Project No. FDK-2019-8750).

Keywords: forest optimization algorithm | genetic algorithm | intensity modulation direct detection OFDM | migrating birds optimization | peak-to-average power ratio | selective mapping

ABSTRACT

In intensity-modulated direct detection optical orthogonal frequency division multiplexing (IM/DD-OOFDM) communication systems, a lower peak-to-average power ratio (PAPR) is essential for improving system performance. In order to reduce the high PAPR, a discrete forest optimization algorithm (DFOA) is integrated with the classical selective mapping (SLM) method in IM/DD-OFDM system. This approach successfully optimizes the values of phase factors, minimizes the search numbers, and reduces computational complexity. To evaluate the impact of the DFOA-SLM method on PAPR reduction, the parameters of the DFOA-SLM method play a crucial role in decreasing the PAPR in an IM/DD optical OFDM system. The DFOA-SLM method demonstrates improved bit error rate (BER) performance, power spectral density (PSD), and power saving performance compared with other PAPR reduction methods. Numerical results indicate that the proposed PAPR reduction method outperforms existing other methods for optical OFDM signals. Specifically, by implementing this technique in the IM/DD optical OFDM communication system, we achieved a decrease in PAPR from 10.68 to 4.88 dB at a complementary cumulative distribution function (CCDF) of 10^{-3}, resulting in a reduction of 5.8 dB. Additionally, the computational complexity of the DFOA-SLM method shows a 73.63% improvement over the classical SLM method when the search number is set to 512.

1 | Introduction

Optical communication systems are developing and improving with time to support high data rate transmission and provide more capacity. Nowadays, wired and wireless communication systems are still suffering from very low security, signal distortion and scattering, and limited bandwidth. Optical communications systems are the best choice for providing these advantages instead of wired and wireless communications. Additionally, orthogonal frequency division multiplexing (OFDM) technology is a popular and attractive technique that supports high data rate transmission by reducing the effects of interference and noise [1]. The OFDM function first divides a high-input information stream into various low information rate streams and then transmits signals by orthogonally placing the sub-carriers. An OFDM is a modulation method used in optical communication topologies to minimize the impact of inter-symbol interference (ISI) while maintaining high data communication speeds and bandwidth. Optical OFDM systems includes a high peak-to-average power ratio (PAPR), which causes the LED source to clip the optical signal, resulting in significant distortion. Various solutions have

been suggested to minimize PAPR, including partial transmit sequence (PTS), clipping and filtering, selective mapping (SLM), and coding [2]. The clipping technique causes in-band distortion by reducing the signal's amplitude to a specified level. Transmitting side information (SI) decreases bandwidth efficiency in the SLM method, while coding techniques significantly reduce PAPR without negatively impacting BER performance [3].

Visible light communication (VLC) technology uses visible LEDs for real-time information transmission at very high speeds. According to [4], it can provide solutions for an extensive range of applications, such as indoor navigation and localization (in situations where current GPS is unavailable) and underground and underwater networks.

Extensive research has been conducted on optical OFDM modulation for VLC systems to facilitate high-speed transmission [5]. An OFDM offers resistance to frequency selective fading channels, power efficiency, a noteworthy high spectral efficiency, and multipath delay spread tolerance. A VLC system relies on IM/DD, requiring both positive and real-valued transmitted signals. VLC systems utilize various types of O-OFDM, such as DC-biased O-OFDM (DCO-OFDM), ACO-OFDM, Flip-OFDM, and ADO-OFDM. A DCO-OFDM network applies a DC bias to the optical OFDM signal to generate a unipolar signal. In ACO-OFDM, data symbols are only carried on odd subcarriers, while even subcarriers are set to zero. In the Flip-OFDM transmission method, the negative and positive halves of the bipolar OFDM signal are transmitted independently over two separate frames. ADO-OFMD combines the features of both DCO-OFDM and ACO-OFDM. Briefly, the subcarriers are categorized as even and odd. ACO-OFDM uses the odd subcarriers, whereas DCO-OFDM uses the even subcarriers [6]. In [7], the authors developed and simulated a 100 Gbps long haul IM/DD OFDM system using Optisystem software, ensuring high data rate for downstream signals.

The transmitted signal must be clipped to zero to create a real and positive signal in ACO-OFDM [8]. However, designing OFDM systems still presents challenges. One of the most significant difficulties is the high PAPR of optical OFDM signals. The PAPR, determined by the total of orthogonal subcarriers generated by the IFFT process at the transmitter, is the maximum to average power ratio. The non-linear characteristics of the LED in the transmitter cause the OFDM signal to shift, requiring a reduction in PAPR to prevent signal cutting and poor BER performance. Numerous PAPR reduction strategies have been described for optical OFDM signals [9]. In [10], the researchers presented a PAPR minimization strategy for clipping that suffers from BER. In [11], the authors reduced the PAPR of the transmitted OFDM signal by recurrent clipping and filtering methods. Some PAPR reducing methods were investigated as amplitude clipping and filtering, SLM, and PTS by Rana et al. in [12]. The authors in [13] studied PTS, SLM, TR, and PI as PAPR reduction methods. The authors in [14] conducted a comparison of PAPR reducing strategies in FBMC and OFDM topologies. In [15], the researchers introduced a machine learning (ML) strategy to reduce PAPR. In [16], the authors applied a modern swarm intelligence optimization algorithm based on the PTS technique to an optical CO-OFDM communication system, and they found that DIWO based on PTS achieved the best performance in reducing PAPR in terms of the BER performance.

Prasad and Arun [17] developed a Hanowa matrix-based approach that improved the performance of the C-SLM method for reducing PAPR. Researchers in [18] have suggested an enhanced PTS PAPR reduction method that decreases BER and power spectral density (PSD) based on moth flame optimization. The authors in [19] have offered a method for reducing PTS PAPR based on m-arrangement. In [20], a two-step (TR) method for reducing PAPR was proposed.

In 2022, fuzzy neural networks were used to propose an adaptive PTS strategy to decrease PAPR in an OFDM system [21]. The ICF method [22] was simulated using three ways to minimize PAPR in an OFDM communication system. Sivadas [23] analyzed PAPR reduction in OFDM systems using the Hadamard-SLM approach. Authors in [24] have proposed using the SLM method with new symmetric Hankel matrices as phase factor series for PAPR minimization in OFDM networks. In [25], the proposed improved PTS technique with Mu-Law companding for PAPR minimization in OFDM systems improves performance in division and phase rotation stages. Mayakannan et al. [26] propose a neural network and linear regression method for PAPR reduction, achieving 84.1% reduction for 16QAM and 82.9% minimization for 64QAM-OFDM, without compromising BER.

An improved PAPR reduction method has been suggested in 2021 using a quantum GA and PTS, resulting in a 64% reduction in computational complexity [27]. Zou et al. reported a technique using neural networks for PAPR reduction, which is based on simplified clipping and filtering (SCF) techniques [28]. In [29], a method was presented for reducing the PAPR using a combination of mixed companding and clipping techniques. In [30], the authors provide an overview of PAPR reduction techniques for three popular modulation schemes in optical and wireless communication systems: O-OFDM, optical-filter bank multicarrier (O-FBMC), and optical non-orthogonal multiple access (O-NOMA), emphasizing their importance in improving system efficiency. In [31], the integration of OFDM with 5G radio waveforms is gaining attention for VLC systems. However, high PAPR can negatively impact system performance. The authors investigate PAPR reduction algorithms for optical OFDM in VLC systems, analyzing techniques like clipping, SLM, PTS, and companding to ensure efficiency and signal integrity.

In [32], the authors propose a scheme that combines DCO-OFDM with index modulation and convex optimization algorithms to address nonlinear distortion in systems with high PAPRs. This method uses partially activated subcarriers to transmit constellation modulated symbol information and a dither signal.

In [33], the authors explores O-OFDM approaches in VLC systems, focusing on factors like constellation size, data arrangement, power efficiency, computational complexity, BER, and PAPR. The study aims to reduce PAPR in VLC systems by proposing a non-distorting technique called the Vandermonde-like matrix (VLM) precoding technique. This technique is implemented across various O-OFDM approaches, including DCO-OFDM, ADO-OFDM, ACO-OFDM, Flip-OFDM, ASCO-OFDM, and LACO-OFDM.

The SLM technique is a popular PAPR reduction algorithm due to its user-friendly structure and efficient performance without signal distortion. In SLM method, a set amount of phase sequences is generated at random. These sequences are then multiplied by the original data, which is modulated over QAM. The best phase sequence is selected based on the transmission signal with the lowest PAPR [34, 35]. The SLM algorithm requires one IFFT procedure for each randomly generated phase sequence, with the amount of searches increasing as the number of randomly produced phase sequences increases. As a result, SLM's computational complexity approaches extremely high values. Minimum search numbers must be used to find reasonable solutions in order to avoid this undesirable scenario. In order to achieve this, we applied an advanced new method for the optical OFDM system known as a DFOA with SLM (DFOA–SLM). This technique uses DFOA-based phase factors optimization iteratively to achieve better solutions with fewer search values [36].

The primary contributions of our research are:

1. An improved DFOA–SLM was applied to our proposed IM/DD optical OFDM system for the PAPR minimization procedure.
2. The DFOA algorithm has been used to decrease PAPR in the optical OFDM system for the first time.
3. Comparison of PAPR reduction techniques through simulation: classical SLM, GA, MBO, and DFOA based on SLM.
4. The influence of DFOA-SLM parameters was examined on our suggested IM/DD optical OFDM system.

The structure of the rest of the paper is as follows:

- Section 2 outlines the fundamental operating principles of the O-OFDM system and discusses the importance of PAPR.
- Section 3 explains the PAPR reduction method including DFOA-SLM.
- Section 4 describes the modified DFOA algorithm, and Section 5 discusses the DFOA-SLM technique.
- Section 6 presents the simulation results and discussion.
- Section 7 analyzes the computational complexity of each optimization method, and Section 8 includes the conclusion.

The definitions of the abbreviations can be found in Table 1.

TABLE 1 | Abbreviations.

ACO-OFDM	Asymmetrically clipped O-OFDM
ADO-OFDM	Asymmetrically clipped DC-biased O-OFDM
BER	Bit error ratio
CCDF	Complementary cumulative distribution function
CO-OFDM	Coherent detection OFDM
DFT	Discrete Fourier transform
DFOA	Discrete forest optimization algorithm
FFT	Fast Fourier transform
FT	Fourier transform
GA-SLM	Genetic algorithm–SLM
GSC	Global seeding changes
IM/DD	Intensity modulation/direct detection
IFFT	Inverse fast Fourier transform
LM-DDO-OFDM	Linearly mapped DDO-OFDM
LSC	Local seeding changes
MBO	Migrating birds optimization
NLM-DDO-OFDM	Nonlinearly mapped DDO-OFDM
NFC	Number of fitness calculations
OFDM	Orthogonal frequency division multiplexing
OSNR	Optical signal-to-noise ratio
PTS	Partial transmit sequence
PAPR	Peak-to-average power ratio
PI	Peak insertion
QAM	Quadrature amplitude modulation
SCF	Simplified clipping and filtering
SLM	Selective mapping
TI	Tone reservation
VLC	Visible lighting communication

2 | System Description and PAPR Analysis

O-OFDM types can be classified as CO-OFDM or DDO-OFDM, depending on the method of detection. DDO-OFDM can be classified into two types: LM-DDO-OFDM and NLM-DDO-OFDM. NLM-DDO-OFDM systems are intensity-modulation optical OFDM topologies, where the intensity of the transmitted optical signal represents the electrical signal. Examples of this method include optical wireless systems, plastic optical fiber systems, and multimode optical fibers. The IM/DD approach ensures intensity modulation without information loss by requiring a true and positive input signal. The IFFT block's input is subject to limitations such as Hermitian symmetry.

Figure 1 illustrates the block diagram of optical IM/DD OFDM system. The IFFT/FFT block plays a critical role in processing signals for both the transmitter and the receiver, serving as the central component of the system. Traditional FT transmits continuous signals in the time/frequency domain, simplifying signal processing by sampling them in the traditional transformation.

Fast algorithms FFT and IFFT are widely used in digital signal processing applications to get the DFT and IDFT. Optical OFDM systems utilize IFFT for modulation at a transmitter and FFT

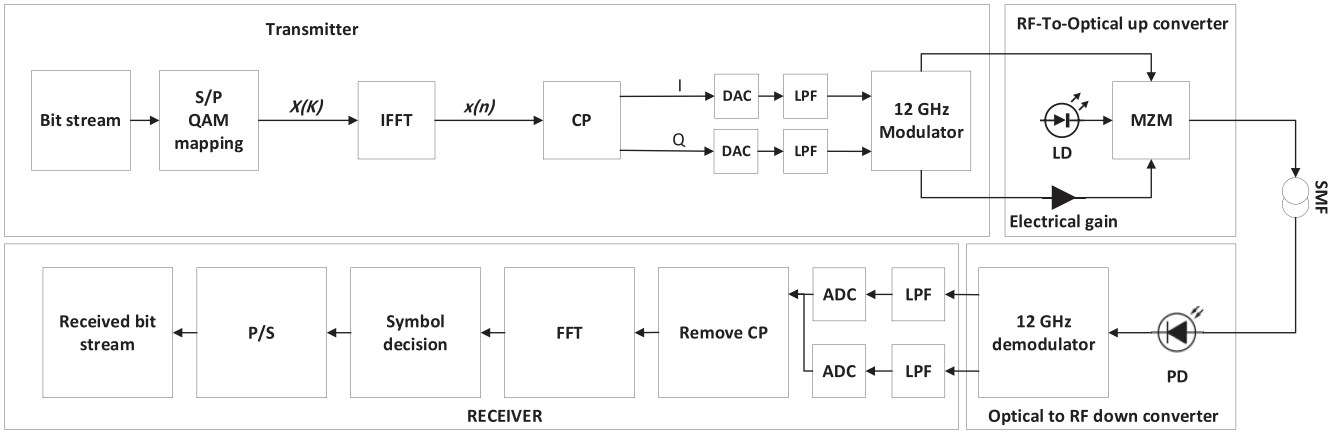

FIGURE 1 | Block diagram of IM/DD optical OFDM communication system.

for demodulation at a receiver. The IFFT is a method that uses a complex input vector as $\boldsymbol{X}=(\boldsymbol{X_0}, \ldots, \boldsymbol{X_{N-1}})$, where $\boldsymbol{X}$ represents the modulated input information sequence, and N represents the total amount of sub-carriers [37].

The modulating signal must be positive and real, so the IFFT block's output is a complex sequence, which is unsuitable for intensity modulation. To satisfy this criterion, the input vector $\boldsymbol{X}$ must be restricted to have Hermitian symmetry. Therefore, the input sequence $\boldsymbol{X}$ is represented as follows [38]:

$$X_i = X^*_{N-i}, \quad 0 < i < \frac{N}{2} \tag{1}$$

where the complex conjugate of $\boldsymbol{X}$ is denoted by $\boldsymbol{X}^*$.

The used subcarriers transposed-conjugate duplicates are inserted into complete the IFFT frame, denoted as $\boldsymbol{X_H}$.

$$X_H = \left[X_0, .., X_{N-1}, X^*_{N-1}, \ldots, X_{N-1}, \ldots, X^*_1\right] \tag{2}$$

and the DC element is $\boldsymbol{X_0 = X_N = 0}$. The transmitted OFDM symbol generates a $2N$-point IFFT output. The discrete OFDM symbol vector outputs, $\boldsymbol{x_k}$, from the IFFT algorithm in the time domain are given by

$$x_k = \frac{1}{N}\sum_{h=0}^{N-1} X_{H,h} e^{j\frac{2\pi hk}{N}}, k = \{0, .., N—1\} \tag{3}$$

h represents the hth sub-carrier symbol of X_H.

Here, $\boldsymbol{x_k}$ is the transmitted OFDM symbol with a period $\boldsymbol{T_p = \frac{1}{\Delta f}}$, where $\boldsymbol{\Delta f = \frac{B}{N-1}}$ is the subcarrier spacing and B is the bandwidth of signal. As a result, a high PAPR remains present in the envelope of the positive and real valued OFDM signal in the time domain [34].

The PAPR of an OFDM signal is the ratio of its peak power to its average power in the time domain as follows:

$$PAPR(dB) = 10\log_{10}\frac{\max|x_k|^2}{E\left\{|x_k|^2\right\}} \tag{4}$$

In this context, $max|\boldsymbol{x_k}|^2$ represents the highest power value of the OFDM signal, while $\boldsymbol{E[.]}$ represents the average of these values. The complementary cumulative distribution function (CCDF) of PAPR is a common statistic that shows a reduction in *PAPR*. It measures how likely it is that the PAPR of an OFDM frame will exceed a certain threshold called $PAPR_0$ [39, 40].

$$CCDF = Prob\left(PAPR > PAPR_0\right) \tag{5}$$

3 | PAPR Reduction Based on the DFOA-SLM Method in the Optical Transmitter

Figure 2 illustrates the schematic diagram of the optical OFDM transmitter after integrating the DFOA-SLM method.

Firstly, the information bits are transformed to different symbols by using any QAM modulation, and the QAM symbols are represented below:

$$X(k) = [X(0), \ldots, X(N-1)] \tag{6}$$

After that, the vector of $X(K)$ is multiplied by the optimized N length different phase rotation factor vectors $\boldsymbol{b^{*(u)}(k)} = \left[\boldsymbol{b^{*(0)}(0)}, ., \boldsymbol{b^{*(u)}(N-1)}\right]$ generated randomly, which $b^{*(u)}(k)$ *including* -1 *and* $1, u = 1, ..., U$. The variable U represents the number of phase factor combinations that are randomly generated. Following the multiplication step, the optimized phase-rotated data sequence symbolized by $X^{(u)}(k)$ is expressed as below:

$$\begin{aligned} \mathrm{X^{(u)}(k)} &= \left[\mathrm{X(0)\times b^{*(u)}(0), \ldots, X(N-1)\times b^{*(u)}(N-1)}\right] \\ &= \left[X^{(u)}(0), , \ldots, X^{(u)}(N-1)\right] \end{aligned} \tag{7}$$

The IFFT operation is applied to the optimized phase-rotated data vector to obtain the following time domain signal:

$$\begin{aligned} \mathrm{x^{(u)}(n)} &= \left[\mathrm{x^{(u)}(0), \ldots, x^{(u)}(N-1)}\right] = \mathrm{IFFT\left(X^{(u)}(k)\right)} \\ &= \frac{1}{\sqrt{N}}\sum_{k=0}^{N-1} \boldsymbol{X(k).\, b^{*(u)}(k).\, e^{j\frac{2\pi k}{N}n}}, \boldsymbol{0 \le n \le N-1, u = 1, \ldots, U} \end{aligned} \tag{8}$$

Then, the candidate OFDM signal with the minimized PAPR is selected to be sent.

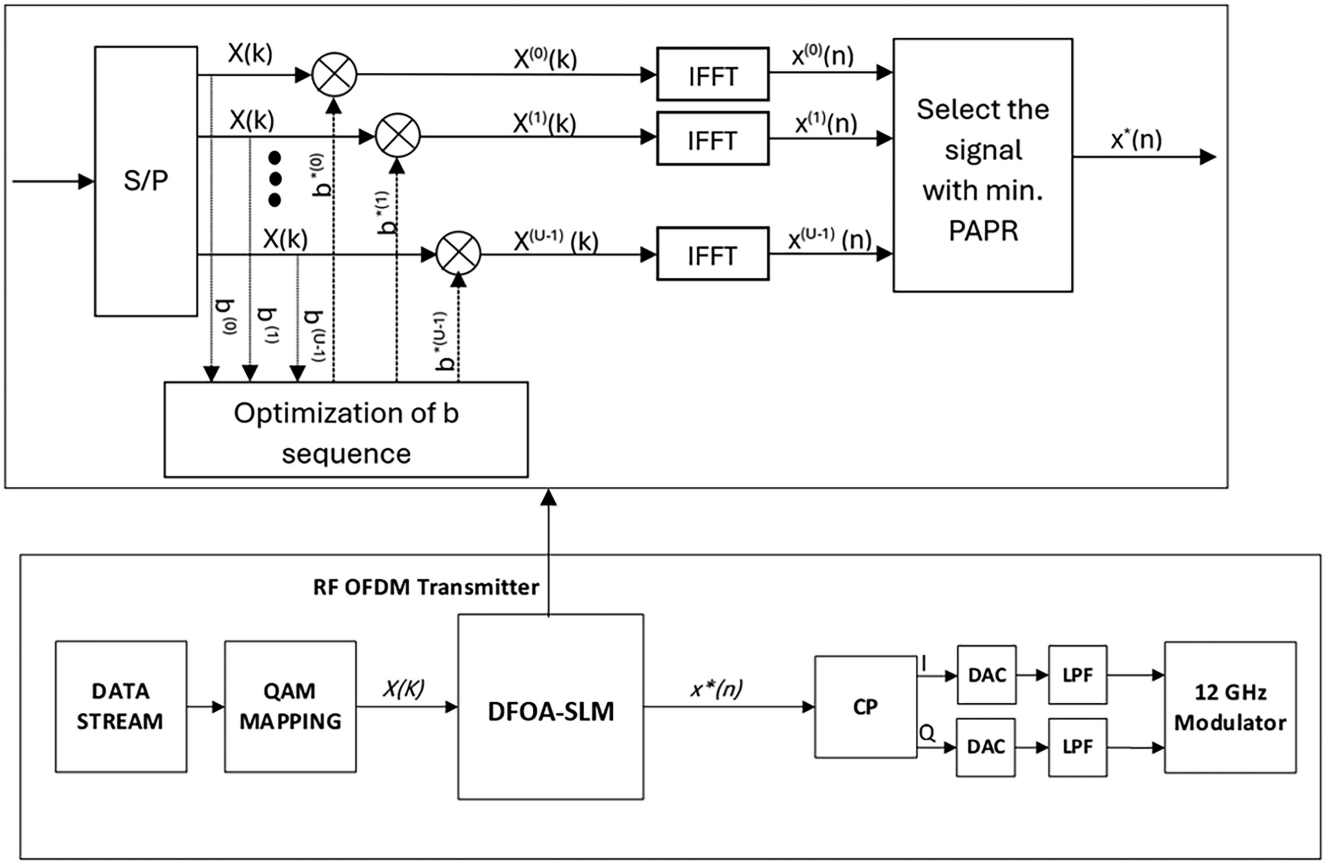

FIGURE 2 | Block diagram of an OFDM transmitter using DFOA-SLM method.

$$x^*(n) = \min_{1 \le u \le U} \left\{ x^{(u)}(n) \right\} \tag{9}$$

The receiver should find the data with the appropriate optimized phase rotation sequences $b^{*(v)}(k)$ to recover the transmitted OFDM signals. The simple method involves transmitting the appropriate SI to the receiver for signal recovery.

4 | DFOA

The DFOA comprises five stages, which will be discussed in detail below:

4.1 | Initialization of the Forest

The algorithm is started by producing random trees in a specified quantity. The solution sequences, denoted by trees, are set with random values of 1 or 0, resulting in a total of $(n+1)$ dimensions for each tree in an n-dimensional solution space, with the first age values determined as 0.

4.2 | Local Seeding Process

In the local seeding phase, a zero-aged tree produces a specified amount of neighbor solutions with the age equal to 0. These solutions are inserted into the forest. The process involves selecting a random tree dimension and reversing its value multiple times. Local seeding changes (LSCs) determine the amount of solutions generated from every tree. After the local seeding step, the age value of every solution, eliminating newly merged population individuals, increases by 1.

4.3 | Population Control Process

The population-limiting process involves reducing the dimension of the population to which new individuals are inserted in the local seeding step by neglecting some members of the forest. Two FOA limits, lifetime and area limit, are decisive in this process. The procedure comprises two elimination steps. The first step is to remove trees older than the lifetime parameter set for the forest. A distinct solution group, named the candidate population, is formed with these elderly individuals for global seeding. The second stage organizes the remaining members of the population based on their fitness values and includes trees that exceed the area limit into the candidate population.

4.4 | Global Seeding Process

The global seeding step involves choosing a percentage of the candidate population from the prior step, adjusted by the transfer rate in the FOA. A random number of dimensions is selected for every tree, controlled by the parameter GSC. The values of

the chosen sizes are varied from 0 to 1 or vice versa. New trees are added to the forest with their age values set to 0.

4.5 | Current Best Tree Updating

The current best solution is determined by sorting population members based on fitness qualities. The tree with the best fitness value is chosen as the current best solution, and its age value is set to 0 to prevent discard due to its age. The procedures from 4.2 to 4.5 are reiterated cyclically until the termination condition is satisfied.

5 | DFOA-SLM Technique

The DFOA proposed in [41] for a continuous optimization algorithm was adapted by Ghaemi and Derakhshi in [42] for feature selection. DFOA was adopted to the classical SLM to represent the digital values as positive and negative ones [36]. In the DFOA-SLM method, phase vectors were not generated randomly to get the optimum solution; DFOA was used to optimize the phase factor sequences that are denoted by the tree locations as below:

$$F^{(t)}(k)=\left[b^{(t)}(0),\ \ldots.,b^{(t)}(N-1),Age^{(t)}\right] \quad \boldsymbol{t}=[\mathbf{1},\ \ldots,\boldsymbol{T}] \tag{10}$$

The variable parameter $\boldsymbol{T}$, which represents the present total amount of trees in the forest, might change during algorithm rounds. In the tree population, $\boldsymbol{Age^{(t)}}$ represents the age of $\boldsymbol{t}$th tree $\boldsymbol{F^{(t)}(k)}$. A detailed description of how to use the DFOA to optimize the phase factor sequences in the SLM method is provided in the following step-by-step manner:

Step 1: Firstly, Equation (10) defines the area limit amount of random trees that are generated to initiate the tree population, where $\boldsymbol{b^{(t)}(k)=1\ or\ -1}$. The first value of T equals area limit. The value of $Age^{(t)}$ takes a value of zero for every of the beginning trees.

Step 2: The following formula is used to determine the initial trees' fitness values:

$$\boldsymbol{fit}(F^{(t)}(\boldsymbol{k}))=\max_{0\le n\le N-1}\left[\left|\frac{1}{\sqrt{N}}\sum_{k=0}^{N-1}\boldsymbol{X(k)}.F^{(t)}(k).\boldsymbol{e}^{\frac{j2\pi kn}{N}}\right|^2\right], \quad \boldsymbol{t=1,..,T} \tag{11}$$

Step 3: For every $\boldsymbol{F^{(t)}(k)}$, if $\boldsymbol{Age^{(t)}}$ equals zero, the tree is treated with a local seeding method outlined below:

$$\boldsymbol{L^{(\alpha,t)}(k)=\underset{0\le k\le N-1}{flip}\left[F^{(t)}(k),1\right],\alpha=1,\ \ldots,LSC;t=1,\ \ldots,T} \tag{12}$$

To create a new tree from Equation (12), $\underset{0\le k\le N-1}{flip}\left[F^{(t)}(k),1\right]$ converts the mark of $F^{(t)}(k)$. The flipping technique is performed $\boldsymbol{LSC}$ times on every zero-aged tree, producing $\boldsymbol{LSC}$-unique new trees. The overall amount of new trees that must be produced during the local seeding step for $\boldsymbol{Y}$ parent trees that are ageless is equal to $\boldsymbol{LSC{\bullet}Y}$. The $\boldsymbol{\alpha}$ th seed of the $\boldsymbol{t}$th tree is represented by $\boldsymbol{L^{(\alpha,t)}(k)}$ in Equation (12).

Step 4: The following procedure is used for evaluating new young trees' fitness:

$$\boldsymbol{fit}\left(\boldsymbol{L^{(\alpha,t)}(k)}\right)=\max_{0\le n\le N-1}\left[\left|\frac{1}{\sqrt{N}}\sum_{k=0}^{N-1}\boldsymbol{X(k)}.L^{(\alpha,t)}(k).\boldsymbol{e}^{\frac{j2\pi kn}{N}}\right|^2\right] \quad \alpha=1,\ \ldots,\mathrm{LSC};\mathrm{t}=1,\ \ldots,\mathrm{T} \tag{13}$$

Step 5: The young trees that are produced and identified by $\boldsymbol{L^{(\alpha,t)}(k)}$ are added to the overall population. The total sum of trees is given by $T=LSC*Y+(area\ limit)$. The ages of the remaining population elements are then raised by one, while those of the young trees are made zero.

Step 6: Older individuals whose ages exceed the lifetime constraint are selected from the existing tree population to create a subset of the candidate population.

Step 7: The elements of the rest population with ages less than or equal to the lifetime restriction are arranged according to their fitness. Trees that exceed the area limits are removed from the forest during sorting, resulting in a candidate population that complies with the area restriction. This ensures that the amount of trees is limited to T less or equal to area limit.

Step 8: A selected group of candidates is chosen, and a predefined parameter transfer rate determines the portion involved. Each selected tree undergoes a global seeding process to produce new trees in remote areas of the forest. The process is applied to the $\boldsymbol{G^{(\beta)}(k)}$ sequences, with the chosen trees indicated by $\boldsymbol{G^{(\beta)}(k)}$ and their total number as $\boldsymbol{B}$.

$$\boldsymbol{G^{(\beta)}(k)=\underset{0\le k\le N-1}{flip}\left[C^{(\beta)}(k),GSC\right],\beta=1,\ \ldots,B} \tag{14}$$

where $\underset{0\le k\le N-1}{\boldsymbol{flip}}\left[\boldsymbol{C^{(\beta)}(k),GSC}\right]$ converts the marks of variable (GSC) various sizes in the $\boldsymbol{\beta th}$ candidate tree denoted by $\boldsymbol{C^{(\beta)}(k)=\left[b^{(\beta)}(0),\ \ldots.,b^{(\beta)}(N-1),Age^{(\beta)}\right]}$. In the range $\boldsymbol{0\le k\le N-1}$, the associated dimensions are chosen at random. The $\boldsymbol{\beta th}$ new solution produced during the global seeding phase is denoted by $\boldsymbol{G^{(\beta)}(k)}$. The main population is then supplemented with the newly created trees. The highest amount of trees is $\boldsymbol{T}$ less or equal to $\boldsymbol{(B+(area\ limit))}$. The age of the recently added $\boldsymbol{B}$ trees is set to 0 in Stage 8.

Step 9: The final population is arranged by fitness rankings. The best tree's age is reset to 0 to ensure it remains a focus in future optimization iterations.

Step 10: The DFOA-SLM method terminates the algorithm if the maximum amount of fitness evaluations (NFC) is reached, while the optimization procedure continues from Step 3.

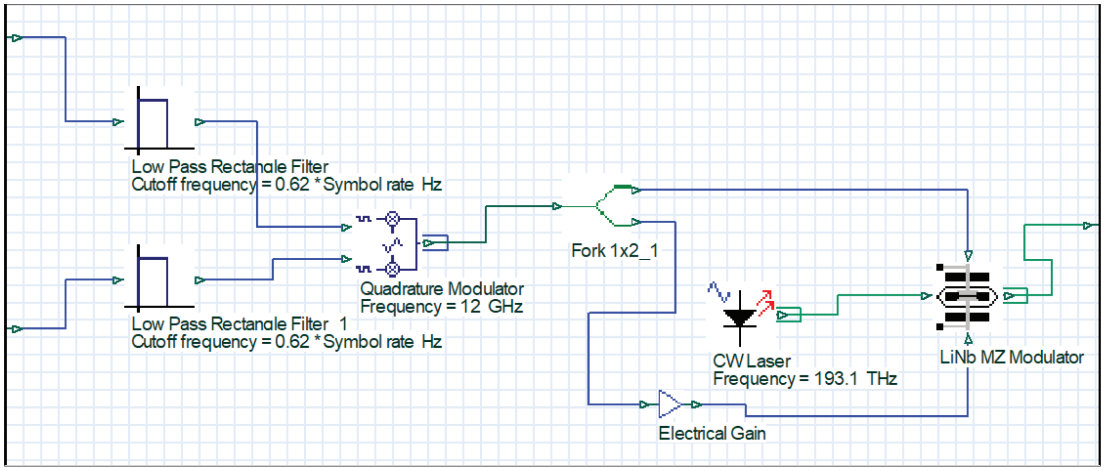

(a)

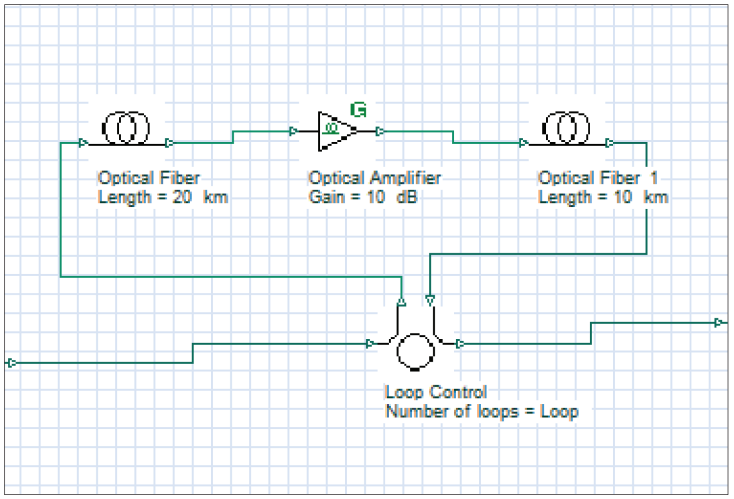

(b)

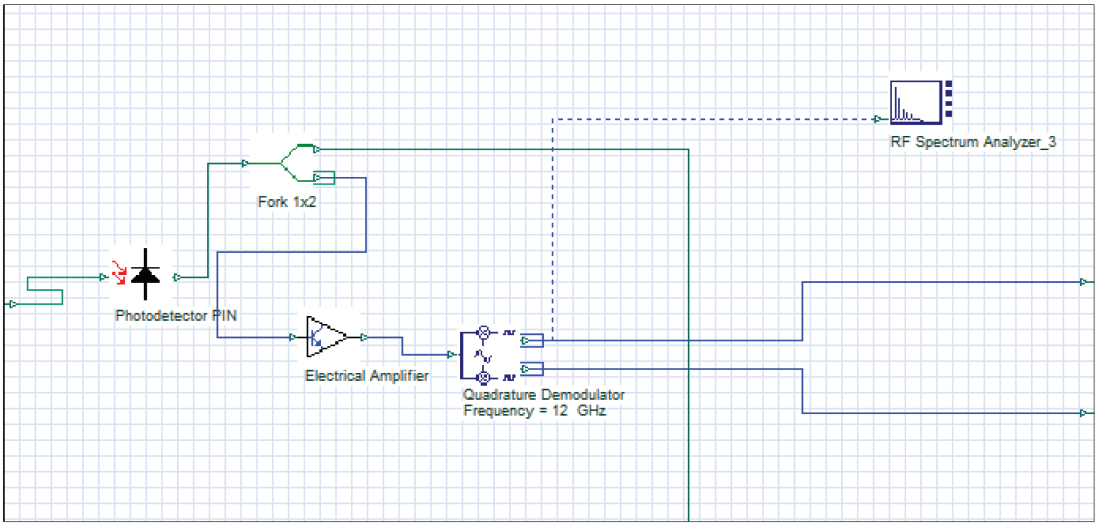

(c)

FIGURE 3 | IM/DD optical OFDM system schematic at OptiSystem software. (a) Transmitter; (b) optical channel; (c) receiver.

6 | Simulation Results and Discussion

Figure 3 illustrates the block diagram of our proposed system. The OptiSystem software was used to simulate the optical system architecture and visualize the results of simulation. As seen in Figure 3, the proposed IM/DD optical OFDM network consists of three basic components: RTO transmitter at CO, optical fiber channel, and OTR receiver at the end user. The global parameters of Optisystem were summarized in Table 2.

The BER test component, with a reference bit rate of 40 Gbps, is used at the transmitter to generate and compare transmitted and received digital bits. It utilizes 128 FFT points and 80 subcarriers. A cyclic prefix of 5 is added after IFFT operation for each OFDM symbol to prevent ISI as summarized in Table 3.

The QAM sequence generator converts generated bits into QAM symbols, which are modulated into several orthogonal subcarriers in an OFDM modulator. However, the subcarriers and FFT point numbers are set to 80 and 128, respectively. The I-Q OFDM signals will be processed through a low pass filter with a cutoff frequency of 12.4 GHz. Quadrature modulators increase the frequency of transmitted OFDM signals to 12 GHz. The transmitted RF electrical signal is converted to the optical field using Mach–Zehnder modulator (MZM). The CW laser and PIN photodetector parameters are listed in Tables 4 and 5, respectively.

Following MZM, the optical signal is sent over ((20 + 10) × no. loops) of single-mode fiber (SMF). DCF reduces the dispersion caused by the primary optical fiber and enhances communication performance. The transmitted signal is amplified by another amplifier within the loop, compensating for any loss. The amplified optical signal is filtered using a filter with a central frequency of 193.1 THz and a BW of 50 GHz. In the receiver, the optical signal is converted into an electrical signal by the photodetector. The electrical signal that is received is amplified by an electrical amplifier. The amplified received signal is demodulated and recovered by a quadrature demodulator. The OFDM modulator and demodulator must have the same parameters to accurately recover QAM symbols. The QAM sequence detector converts these symbols into bits per symbol, and the BER test set evaluates the BER and its logarithm.

The proposed optical OFDM system is designed, analyzed, and simulated for 4-QAM and 16-QAM using Optisystem software, as shown in Figure 3. Figure 4 illustrates the transmitted and the received 4 and 16 QAM symbols at a propagation length of 30 km. The received symbols are correctly recovered because of the short propagation length, as illustrated in Figure 4b.

Figure 5 illustrates the electrical OFDM spectrum of the optical system at 12 GHz after the quadrature modulator and photodetector, respectively. The electrical OFDM signal has a bandwidth of 20 GHz (4-QAM) and 10 GHz (16-QAM), which is determined by the number of bits per symbol, as shown in Figure 5. A quadrature modulator comprises three main parameters to be set up: gain, frequency and bias. The bias is increased to 2 to remove the negative values of the transmitted OFDM signal. In the optical OFDM systems, the transmitted OFDM signal should be positive and real due to the increasing bias of the quadrature modulator.

TABLE 2 | The primary parameters of the simulation.

Global Parameters of Optisystem	Value
Sequence length	262,144
Samples per bit	4
Bit rate	40 Gbps
Number of samples	1,048,576 (4-QAM) 2,097,152 (16-QAM)
Symbol rate	$20e^9$ symbols/s (4-QAM) $10e^9$ symbols/s (16-QAM)

TABLE 3 | The primary parameter values of an OFDM modulator.

Name	Value
FFT points	128
Number of used subcarriers	80
Cyclic prefix	5

TABLE 4 | The parameters of a CW laser.

CW laser parameter	Value
Optical frequency	193.1 THz
Output power	1.25 mW
Line width	0.01 MHz

TABLE 5 | Parameters of the PIN photodetector.

PIN photodetector parameter	Value
Dark current	10 nA
Responsivity type	InGaAs

Figure 6a shows the OFDM optical spectrum after the LiNb MZ Modulator, with fundamental values like 30 dB extinction ratio, 4 V switching RF voltage, and 2 V bias voltage. MZM converts the modulated electrical signal to the optical domain after injecting a CW laser with a frequency of 193.1 THz. The optical OFDM signal is transmitted via an optical fiber with two fiber lengths and one optical amplifier. Figure 6b illustrates the received optical OFDM spectrum before passing through the PIN photodetector. The Gaussian optical filter, which helps to reduce noise in the optical channel, is located between it and the receiver. The frequency of a Gaussian optical filter is 193.1 THz, and its bandwidth is 50 GHz.

In Figure 7, we visually analyze the performance differences among three techniques for reducing PAPR by presenting the $PAPR_0[dB]–CCDF$ curves for each method. The results indicate that both the GA and the MBO methods based on the SLM technique improve PAPR minimization performance compared

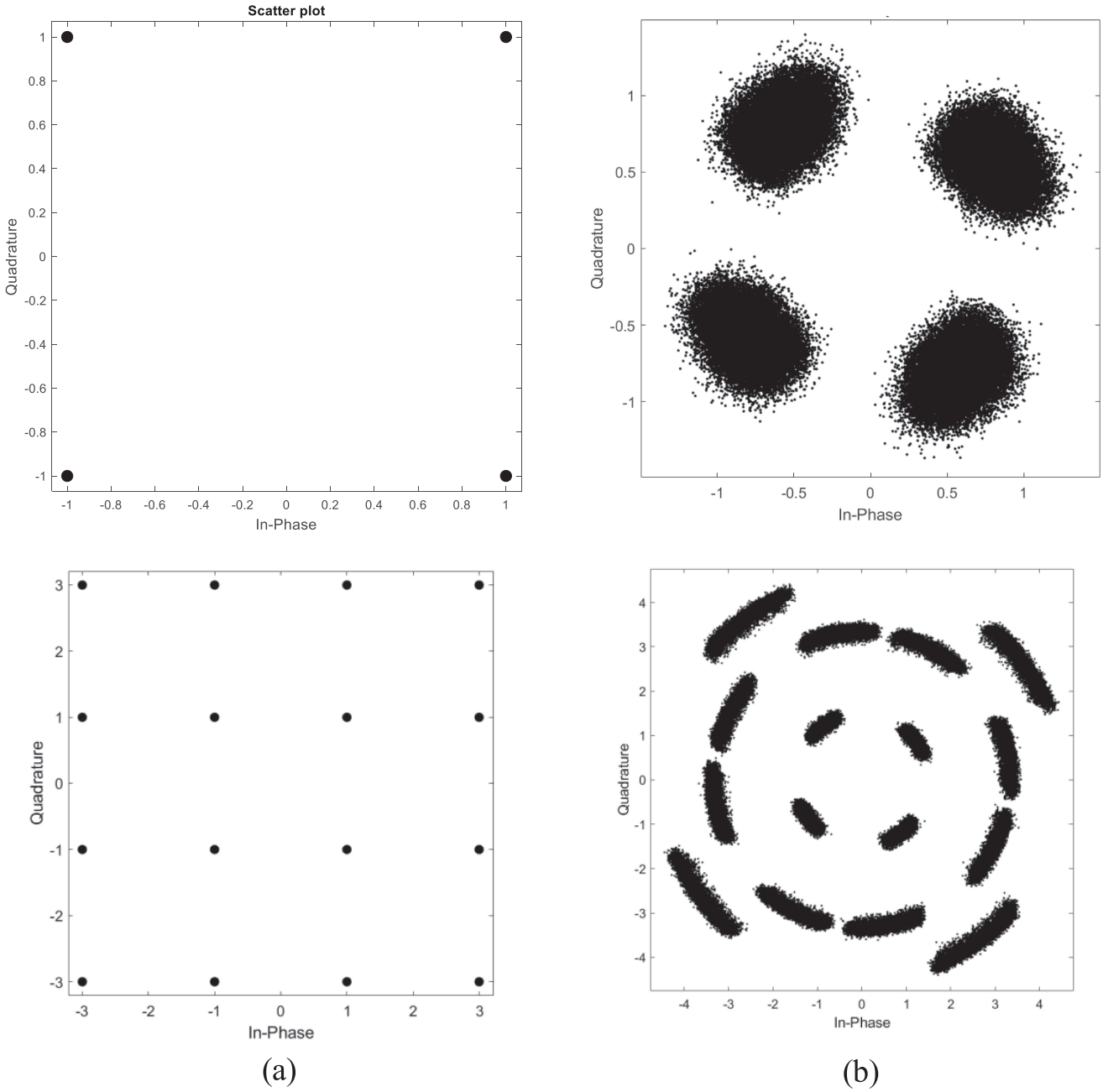

FIGURE 4 | The constellation diagram of (a) transmitted and (b) received symbols.

with the classical SLM technique. However, the most significant enhancement is achieved with the DFOA-SLM strategy. At a CCDF of 10^{-3}, the DFOA-SLM method outperforms the MBO-SLM by 0.09 dB and provides PAPR improvements of 0.5 and 0.68 dB over the traditional SLM and GA-SLM methods, respectively.

In Table 6, the search complexity equations obtained for each of the SLM-based PAPR minimization techniques and the PAPR values reached at CCDF of 10^{-3} if the search complexity of the techniques is equal to 512, are given in the second and third columns, respectively. The parameters for each optimization method are detailed in Table 7, based on an *SN* of 512.

Figure 8 examines the impact of various modulation orders on the performance of DFOA-SLM and other PAPR minimization techniques, analyzing the PAPR curves for 4 and 16 QAM, respectively. Figure 8 shows that the modulation scheme decreases from 16 to 4-QAM results in minimal improvements in DFOA–SLM, MBO–SLM, GA–SLM, and the traditional SLM scheme. The PAPR reductions in DFOA–SLM, MBO–SLM, GA–SLM, and classical SLM techniques at CCDF 10^{-3} are 0.029, 0.0404, 0.012, and 0.007 dB, respectively.

Additionally, various high-order M-QAM modulation was tested, including 32-QAM, 64-QAM, 128-QAM, and 256-QAM, utilizing various PAPR reduction methods applied to our proposed IM-DD optical OFDM system to illustrate the CCDF of the PAPR performance under the DCF-SMF channel. Figure 9 shows the CCDF performance of the optical OFDM for 32-QAM in the DCF-SMF channel. At a CCDF of 10^{-3}, the DFOA-SLM approach has a minimum PAPR of approximately 4.84 dB,

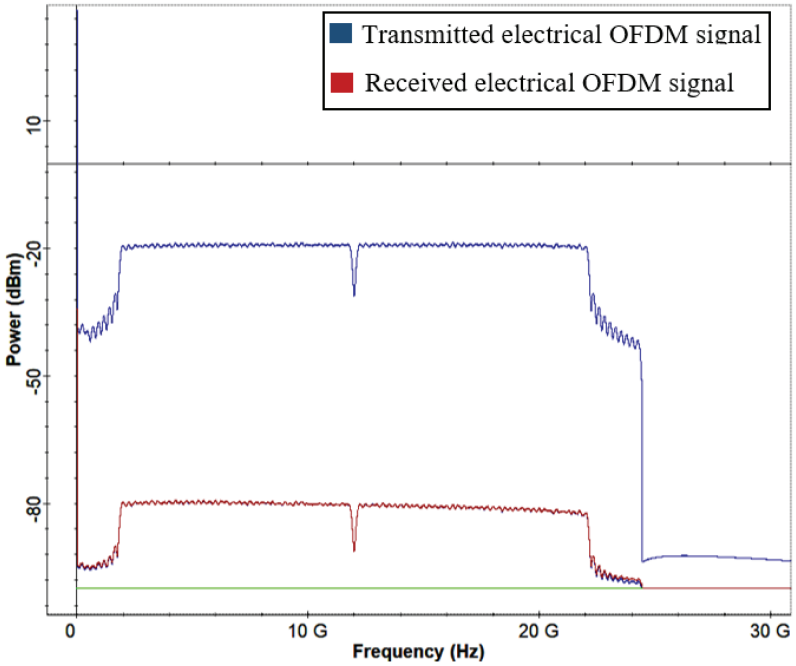

(a)

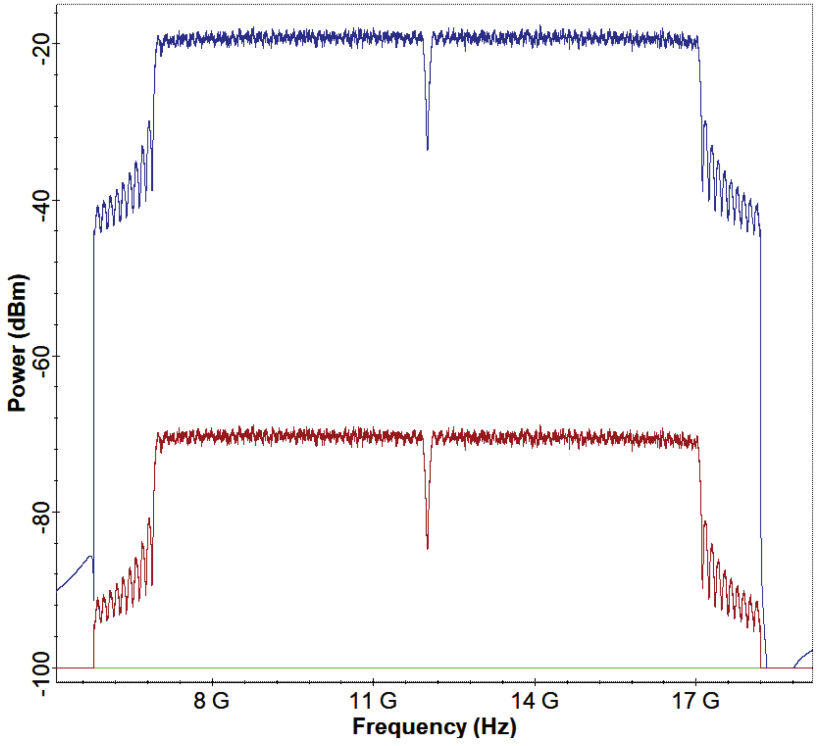

(b)

FIGURE 5 | Transmitted and received electrical OFDM signal for (a) 4-QAM and (b) 16-QAM.

followed by MBO-SLM (5.02 dB), GA-SLM (5.36 dB), SLM (5.53 dB), and optical OFDM, with no PAPR reduction, reaching up to almost 10.10 dB.

Figure 10 shows the CCDF performance of the optical OFDM for 64-QAM in the DCF-SMF channel. At a CCDF of 10^{-3}, the proposed DFOA-SLM algorithm has a minimum PAPR of around 4.86 dB, followed by MBO-SLM (5.03 dB), GA-SLM (5.38 dB), SLM (5.55 dB), and optical OFDM, with no PAPR reduction, reaching up to almost 10.22 dB.

Figure 11 illustrates the CCDF performance of optical OFDM for 128-QAM in the DCF-SMF channel. At a CCDF of 10^{-3}, the proposed DFOA-SLM algorithm achieves a minimum PAPR of

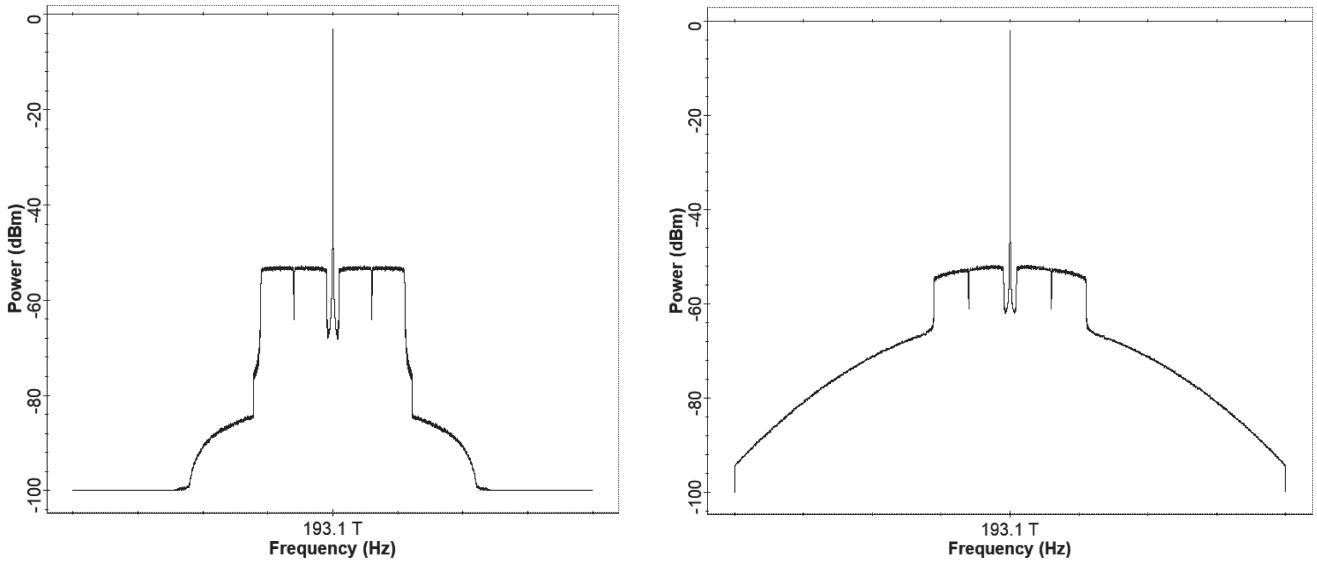

FIGURE 6 | The transmitted optical OFDM signal before (a) the optical channel and before (b) the PIN photodetector.

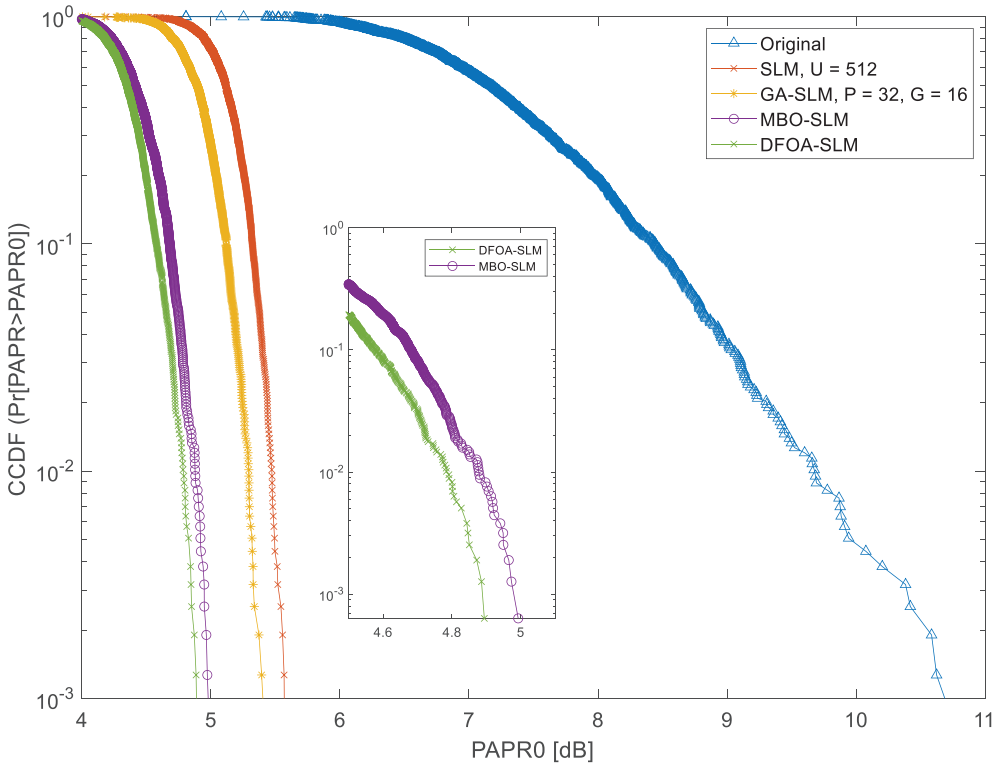

FIGURE 7 | Comparison of the DFOA-SLM technique with the considered optimization methods regarding their PAPR reduction performance.

approximately 4.87 dB, followed by the MBO-SLM at 5.04 dB, GA-SLM at 5.39 dB, SLM at 5.56 dB, and the optical OFDM, which exhibits no PAPR reduction, reaching nearly 10.77 dB.

Figure 12 presents the CCDF performance of optical OFDM for 256-QAM in the DCF-SMF channel. At a CCDF of 10^{-3}, the proposed DFOA-SLM algorithm achieves a minimum PAPR of approximately 4.88 dB, followed closely by MBO-SLM at 5.05 dB, GA-SLM at 5.4 dB, and SLM at 5.57 dB. In contrast, the optical OFDM exhibits no reduction in PAPR, reaching nearly 10.79 dB.

After applying various M-QAM orders to our proposed IM/DD optical OFDM system, we observed that the performance in reducing PAPR showed minimal variation via the same optical fiber channel as shown from Figure 8 to Figure 12. The effectiveness of PAPR reduction can be influenced by the number of subcarriers and the parameters of each PAPR

TABLE 6 | Search complexity analysis of the considered PAPR reduction schemes.

Methods	Search number (SN)	PAPR (dB)
Original	0	10.68
SLM	U = 512	5.56
GA-SLM	P*G = 32*16 = 512	5.40
MBO-SLM	([(W-H) + W. (F-1)]. T. C) = 512, F = 5; H = 1; W = 4; T = 4; C = 8	4.97
DFOA-SLM	NFC = 512	4.88

TABLE 7 | The parameters of every optimization algorithm when the SN = 512.

Methods	Parameter and its value
GA-SLM	Crossover rate = 0.6 Mutation rate = 0.01
MBO-SLM	Number of initial solutions (F) = 5; Number of neighboring solutions to be assumed (W) = 4; Number of neighboring solutions to be shared with the following solution (H) = 1; Number of tours (T) = 4; Number of cycles (C) = 8
DFOA-SLM	Lift time = 2 Transfer rate = 20 GSC = 1 LSC = 2 Area limit = 5

reduction algorithm. A lower PAPR improves power amplifier efficiency, reduces non-linear distortion, and increases system reliability.

Figure 13 provides a detailed depiction of the measured received power for 4 and 16-QAM OFDM signal, both with and without the implementation of the DFOA-SLM technique, under two distinct scenarios: back-to-back (BTB) connections and a 30-km DCF–SMF communication system. In this experiment, the power of the CW laser (P_t) was systematically varied from 0 to 10 dBm to evaluate the impact of the proposed optimization algorithm on the received power. The results illustrated in Figure 13 indicate a notable improvement in power performance following the application of the proposed DFOA-SLM technique. Specifically, an impressive improvement of up to 8 dB in power penalty was recorded at a transmitted power level of 5 dBm. This significant advancement demonstrates that the DFOA-SLM technique plays a critical role in boosting the overall performance of the IM/DD optical OFDM system, primarily by effectively reducing the PAPR.

Figures 14–18 illustrate how different parameters of the DFOA impact the PAPR reduction performance of the DFOA-SLM technique. Each figure focuses on a single DFOA parameter within a specified range, while the other parameters are held constant. Detailed values for the fixed parameters can be found in the explanation section of Table 6. In Figure 14, we examine the effects of changing the field limit parameter on the performance of the DFOA based on SLM technique. Three different area limit weights were tested to identify which ones resulted in better PAPR reduction performance. The results, displayed in Figure 14, show that increasing the area limit parameter from 5 to 25 led to a consistent decline in the PAPR reducing performance of the proposed technique (DFOA based on SLM). Specifically, when the area limits were set to 5, 15, and 25, the

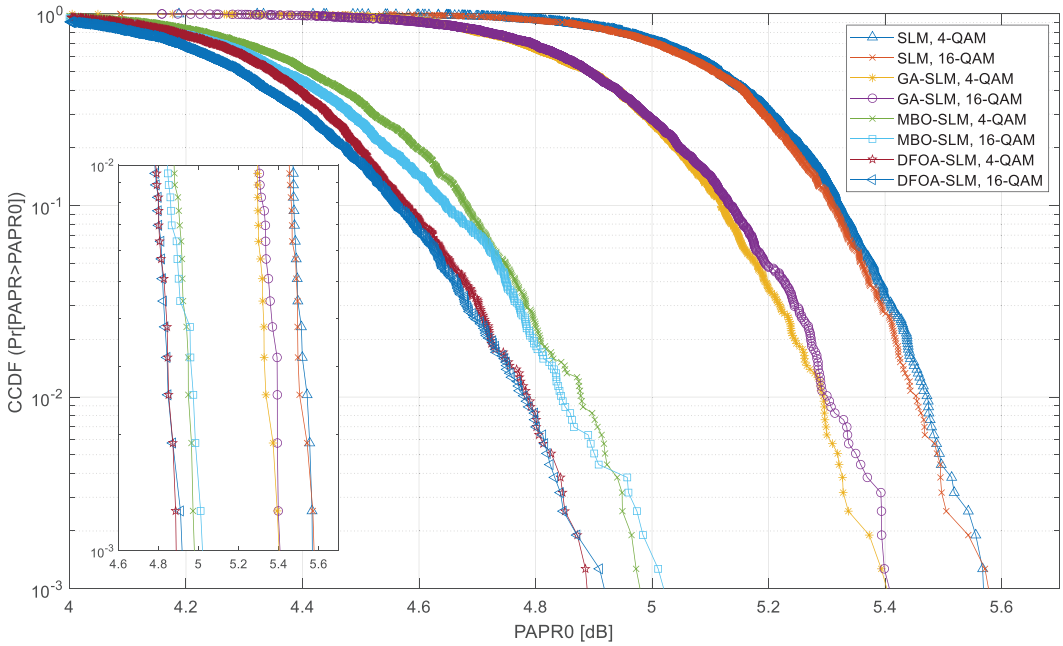

FIGURE 8 | PAPR reducing performance of the DFOA-SLM, MBO–SLM, GA–SLM and the classical SLM technique for 4 and 16-QAM orders.

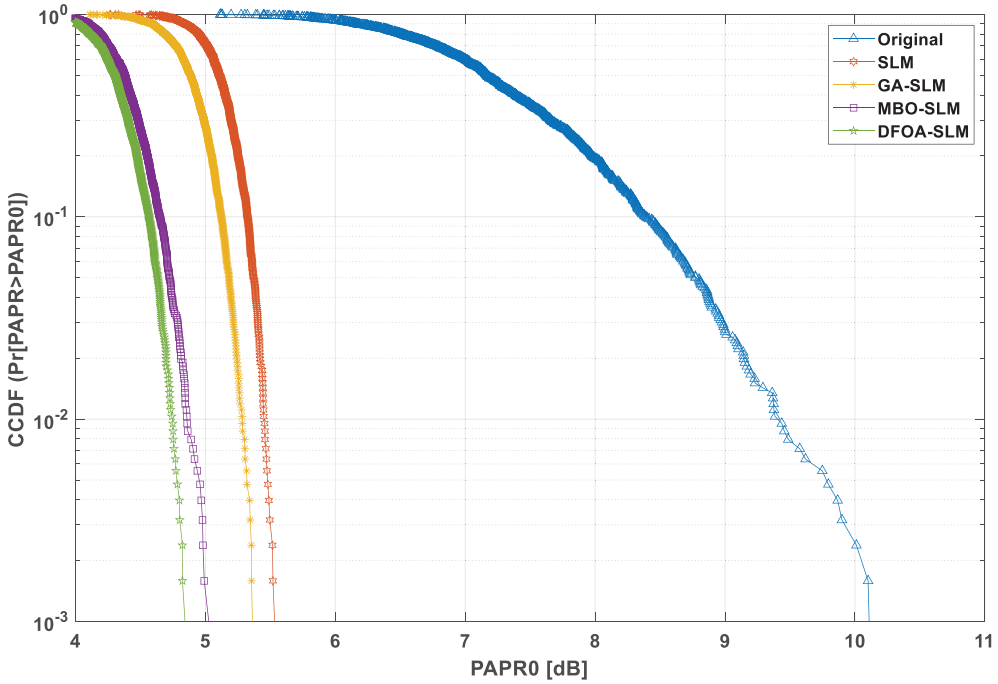

FIGURE 9 | PAPR performance of optical OFDM on the DCF-SMF channel for the 32-QAM modulation.

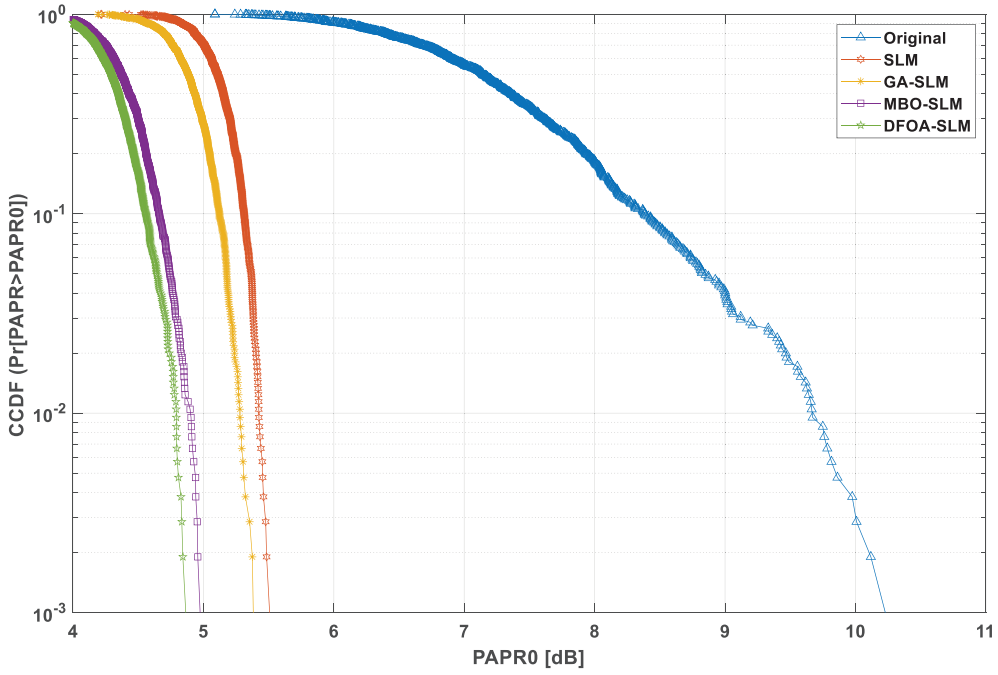

FIGURE 10 | PAPR performance of optical OFDM on the DCF-SMF channel for the 64-QAM modulation.

resulting PAPR values at a CCDF of 10^{-3} were 4.92, 4.96, and 5.04 dB, respectively.

In Figure 15, the lifetime parameter is varied from 1 to 8 to evaluate its effect on the DFOA-SLM strategy's performance. Testing across this range revealed that, except for the values of 1 and 2, lifetime values from 3 to 8 had little impact on PAPR reduction performance.

For instance, when the lifetime parameter was set between 3 and 8, the maximum variation in PAPR at a CCDF of 10^{-3} was only 0.04 dB. In contrast, the poorest and best PAPR reduction performances were achieved with the lifetime parameter values of 1 and 2, respectively.

In Figure 16, the proposed reduction technique is evaluated at five different transfer rate values, which increase in increments of 5 up to a maximum of 40. The PAPR [dB]–CCDF curves shown in Figure 16 indicate that the most effective PAPR reductions were achieved with transfer rates of 15, 20, and 30. Among these, the optimal transfer rate that maximizes the performance of the proposed method (DFOA-SLM) is 20.

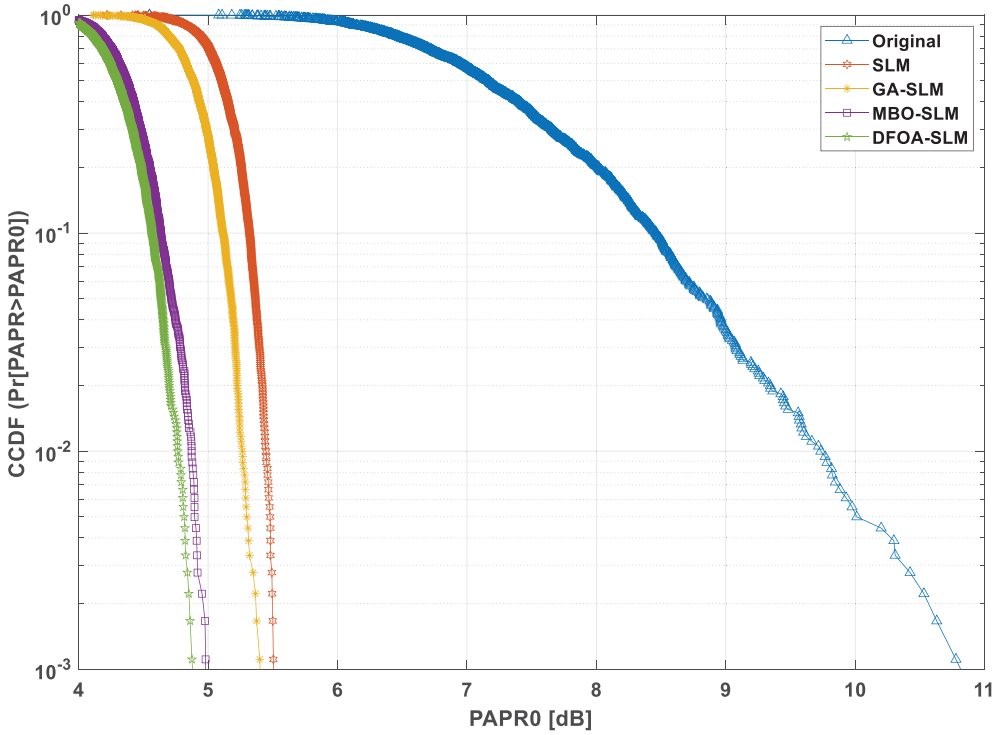

FIGURE 11 | PAPR performance of optical OFDM on the DCF-SMF channel for the 128-QAM modulation.

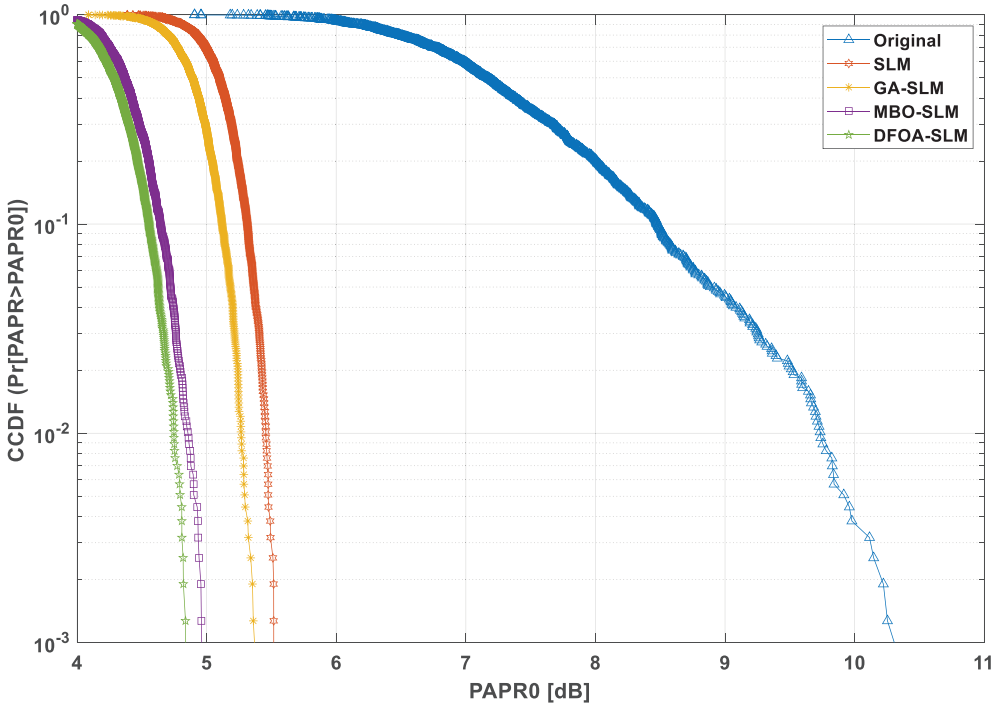

FIGURE 12 | PAPR performance of optical OFDM on the DCF-SMF channel for the 256-QAM modulation.

For example, at a CCDF = 10^{-3}, the PAPR values observed were 4.93 dB for a transfer rate of 5, 4.95 dB for 15, and 4.91 dB for 30. Conversely, transfer rates higher than 30 resulted in a significant decline in the DFOA-SLM strategy's performance. Specifically, for a transfer rate of 40, the PAPR found by the proposed method (DFOA based on SLM) at a CCDF of 10^{-3} was 5.21 dB.

In Figure 17, the performance of the DFOA-SLM method in decreasing PAPR is evaluated for different ***LSC*** values. Upon careful examination of the figure, it becomes apparent that the *PAPR* curves for six various (***LSC)*** values can be categorized into two distinct sets based on the horizontal axis. The first group, corresponding to ***LSC*** values of 1, 2, and 3, shows one pattern of PAPR reduction, while the second group features

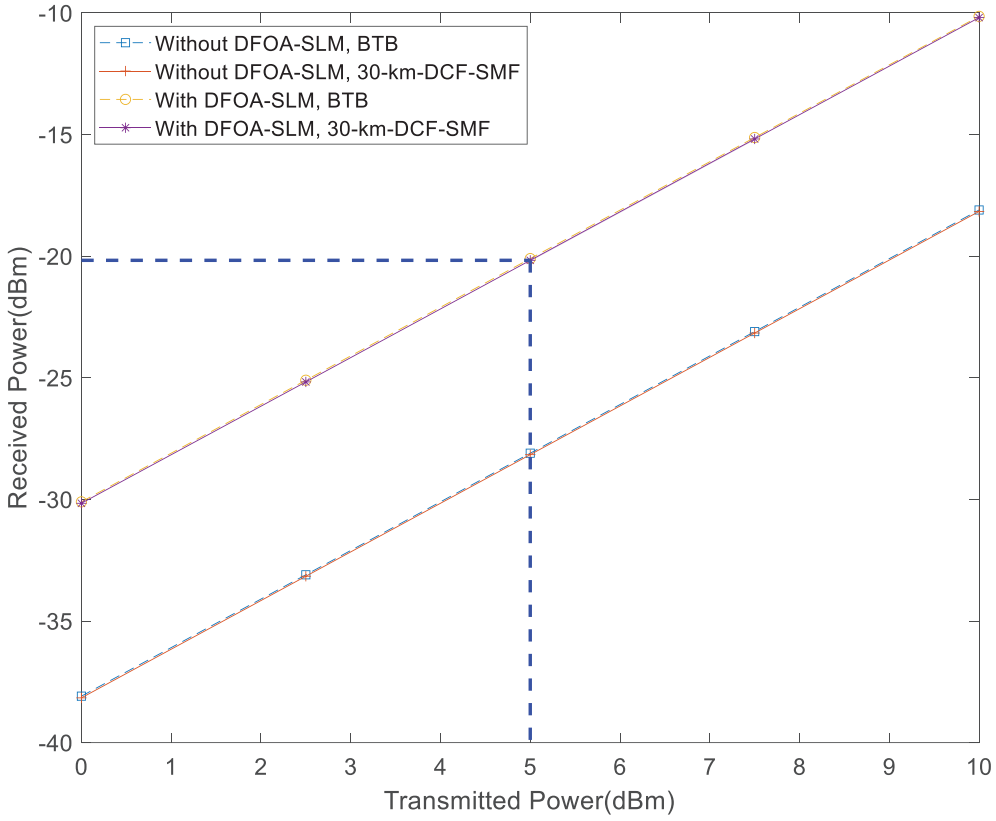

FIGURE 13 | Transmitted power versus the received power of the optical OFDM signal with and without DFOA-SLM technique.

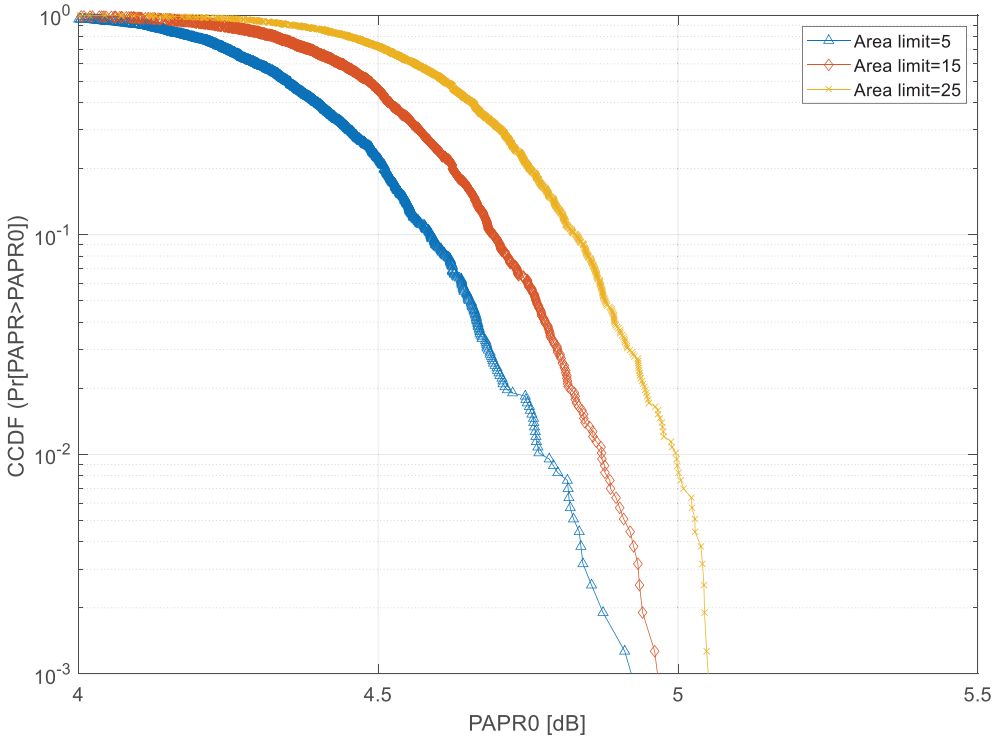

FIGURE 14 | Performance of the DFOA based on SLM technique in reducing PAPR for different area limit.

LSC values of 4, 5, and 6, demonstrating a different performance trend. The results indicate that assigning an ***LSC*** value greater than 3 significantly deteriorates the PAPR reducing performance of the proposed algorithm. Notably, the most effective PAPR curve within the first set is achieved with an ***LSC*** value of 2. When examining the PAPR values obtained at

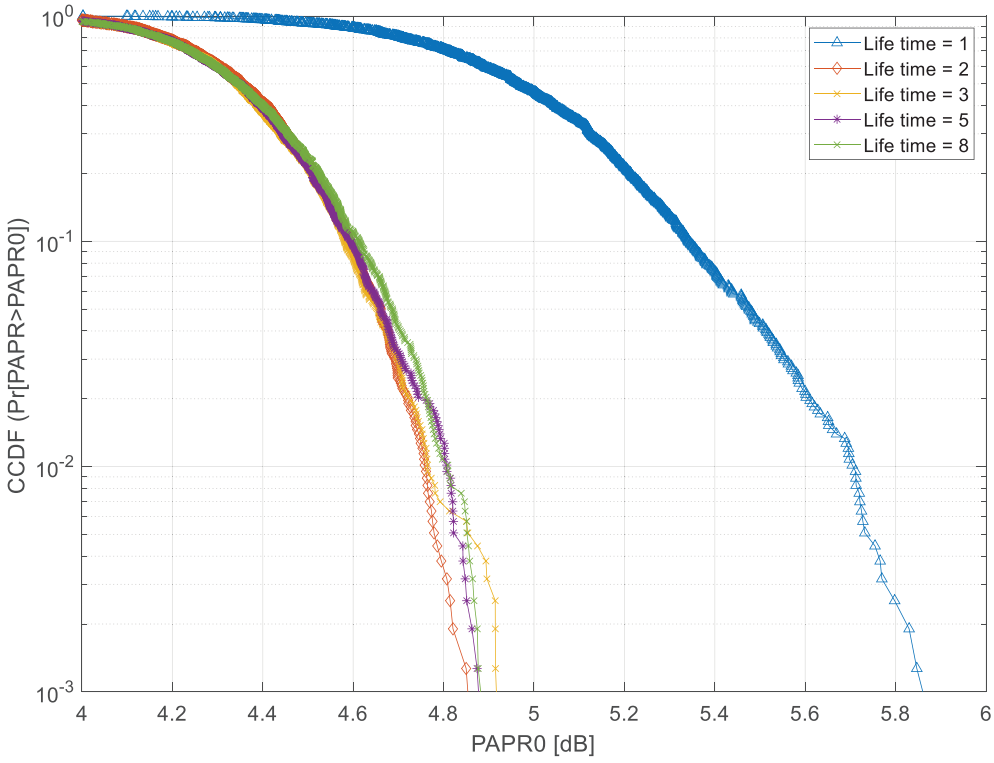

FIGURE 15 | PAPR curves obtained by the DFOA based on SLM technique for different values of the lifetime variable.

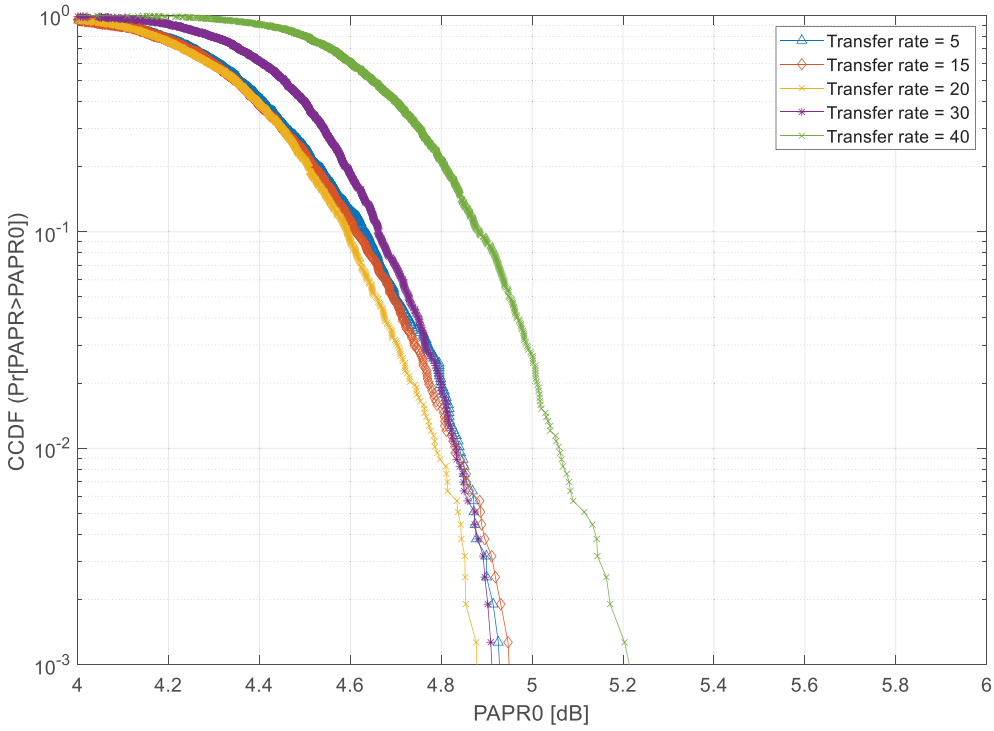

FIGURE 16 | The effect of transfer rate on the performance of the suggested PAPR reduction method.

a CCDF of 10^{-3} in Figure 17, the DFOA-SLM technique yields PAPR values of 5.08, 4.96, and 4.90 dB for the (***LSC***) variable values of 1, 2, and 3, respectively.

In Figure 18, a sequence of (***GSC***) values starting from 1 to 6 were applied to examine how different (***GSC)*** variable values impact the PAPR decreasing performance of the suggested reduction method (DFOA based on SLM). Six distinct PAPR0 [dB]–CCDF curves were generated, each corresponding to a different GSC value. The results, as shown in Figure 18, indicate that increasing the GSC value from 1 to 6 results in a consistent decline in the PAPR decreasing performance of the

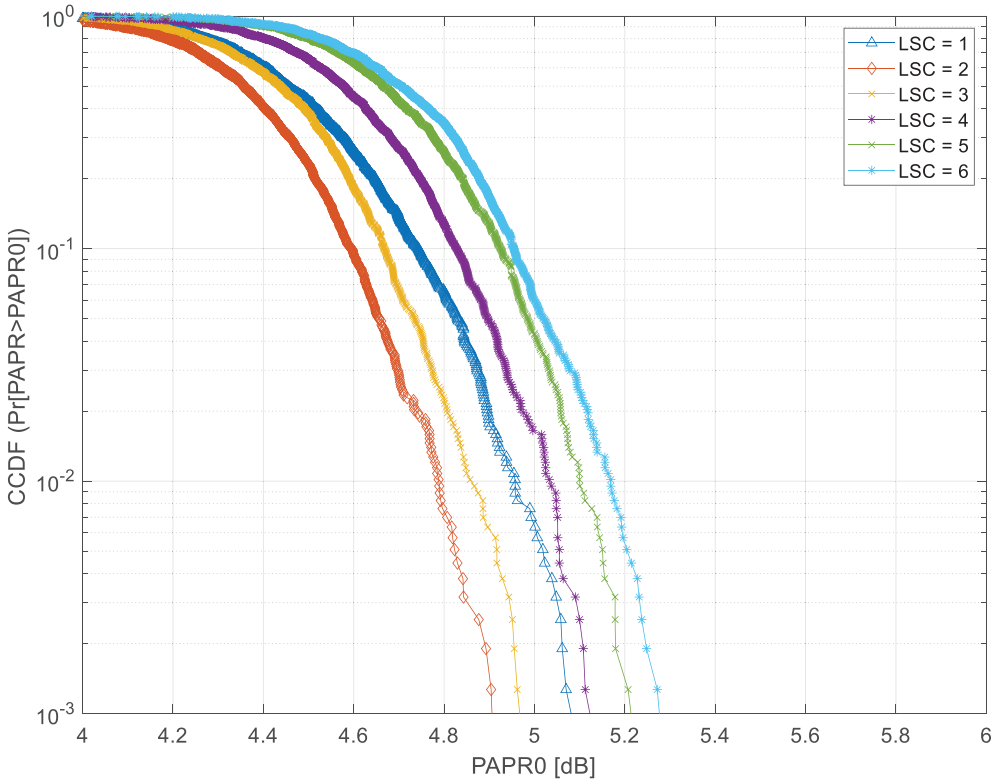

FIGURE 17 | Performance analysis of the proposed method (DFOA-SLM) for various ***LSC*** values.

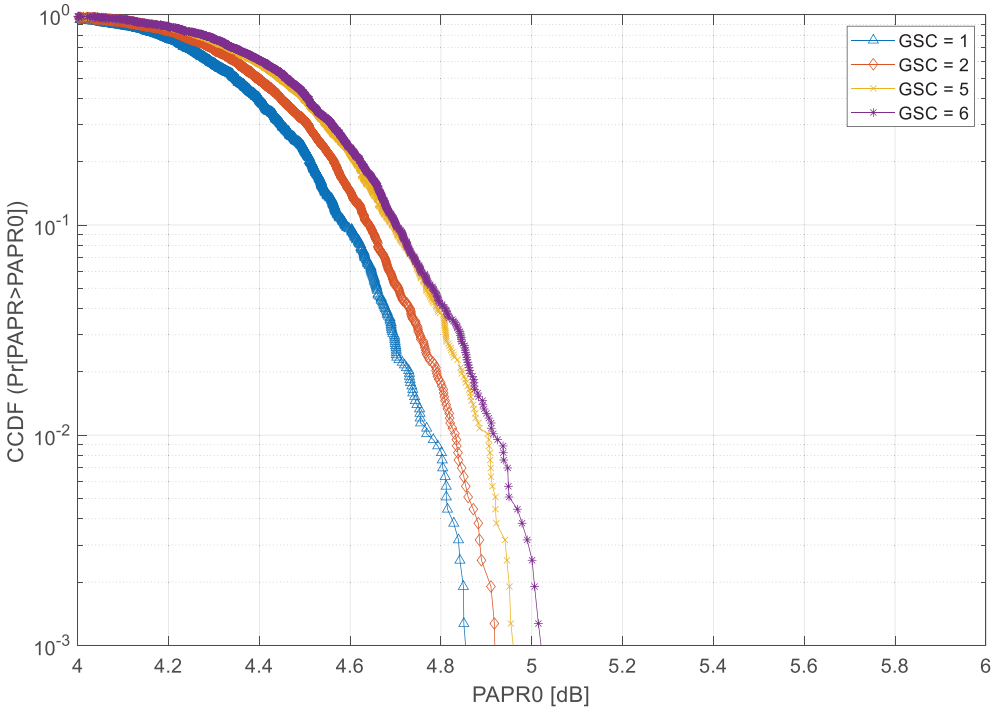

FIGURE 18 | Effect of various ***GSC*** values on PAPR reduction performance of DFOA-SLM algorithm.

suggested algorithm (DFOA based on SLM). Notably, while the ***GSC*** variable is rising from 1 to 2, the deterioration in PAPR reduction performance is significantly more pronounced. For instance, when the ***GSC*** parameter values are set to 1, 2, 5, and 6, the PAPR values accomplished by the proposed method (DFOA based on SLM) at a CCDF of 10^{-3} are 4.85, 4.91, 4.95, and 5.01 dB, respectively.

The overall PSD of the signal is calculated by summing the PSDs of all individual subcarriers. Because the subcarriers are

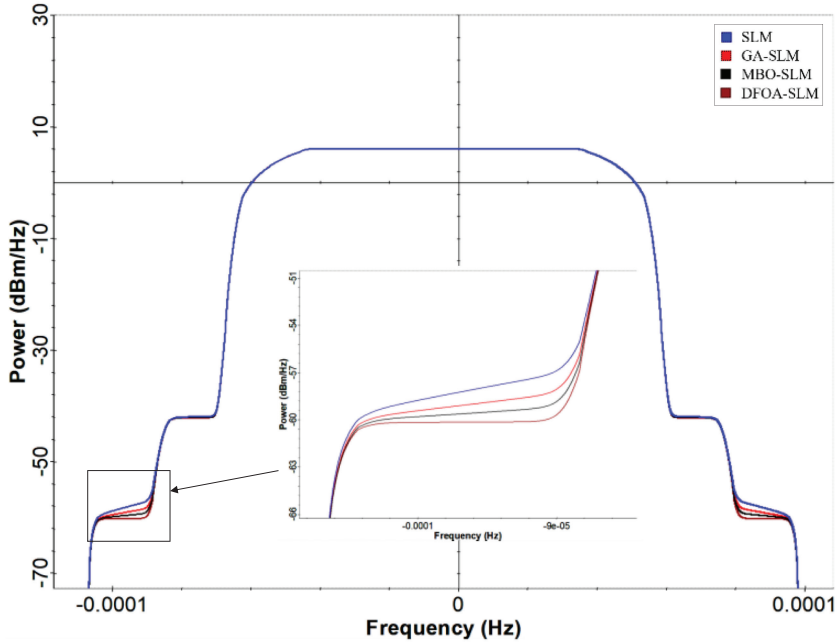

FIGURE 19 | PSD analysis of optical OFDM spectrum after using PAPR reduction methods for the 4-QAM modulation.

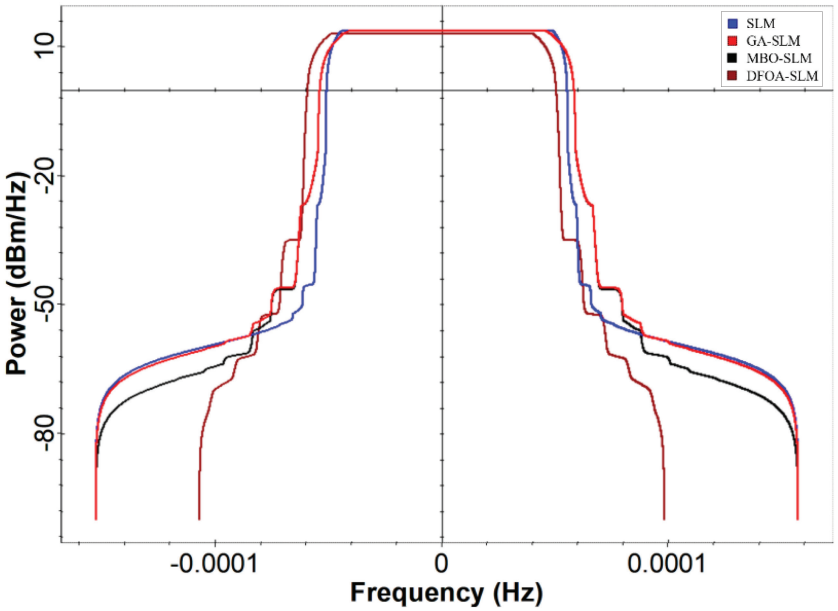

FIGURE 20 | PSD analysis of optical OFDM spectrum after using PAPR reduction methods for the 16-QAM modulation.

orthogonal, their power contributions combine constructively, leading to a flat overall PSD across the frequency range they occupy. The flat PSD shows a uniform power distribution across the subcarriers, effectively utilizing the available spectrum. Figure 19 illustrates the PSD of the O-OFDM waveform, along with the applied PAPR methods for 4-QAM modulation. The increase in sidebands results in significant spectrum leakage within the O-OFDM waveform. It has been observed that PAPR reduction algorithms effectively reduce the spectrum leakage in optical OFDM systems. The spectrum leakage values indicated in the graph are approximately −57 dBm/Hz for SLM, −58 dBm/Hz for GA-SLM, −61 dBm/Hz for MBO-SLM, and −65 dBm/Hz for DFOA-SLM, respectively.

Figure 20 shows the PSD performance of the proposed and classical PAPR techniques for 16-QAM on the optical fiber channel. The spectrum leakage values indicated in the graph are approximately −56.6 dBm/Hz for SLM, −57 dBm/Hz for GA-SLM, −59 dBm/Hz for MBO-SLM, and −60.22 dBm/Hz for DFOA-SLM, respectively.

Figure 21 shows the PSD performance of the proposed and classical PAPR techniques for 32-QAM on the optical fiber channel. The spectrum leakage values indicated in the graph are approximately −49.3 dBm/Hz for SLM, −51.3 dBm/Hz for GA-SLM, −52.6 dBm/Hz for MBO-SLM, and −55 dBm/Hz for DFOA-SLM, respectively.

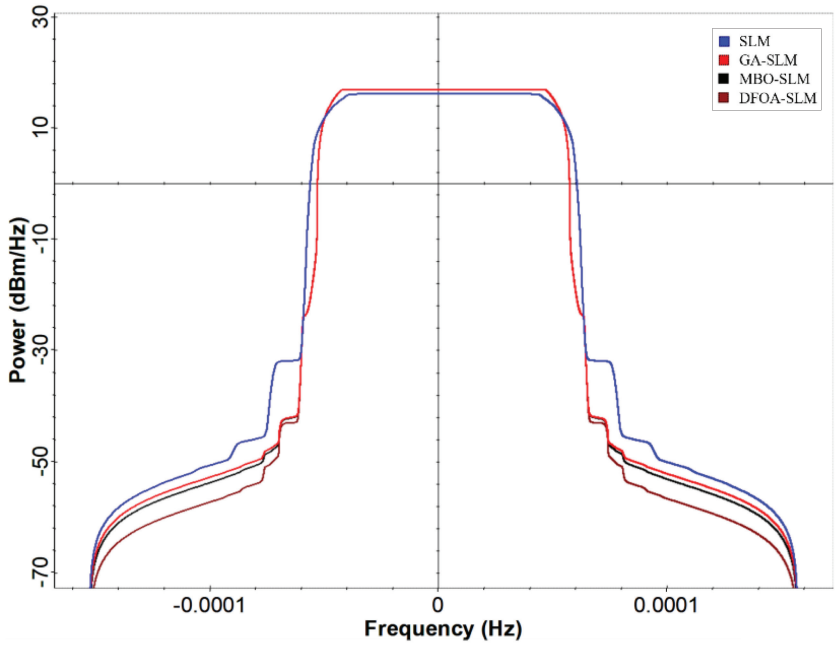

FIGURE 21 | PSD analysis of optical OFDM spectrum after using PAPR reduction methods for the 32-QAM modulation.

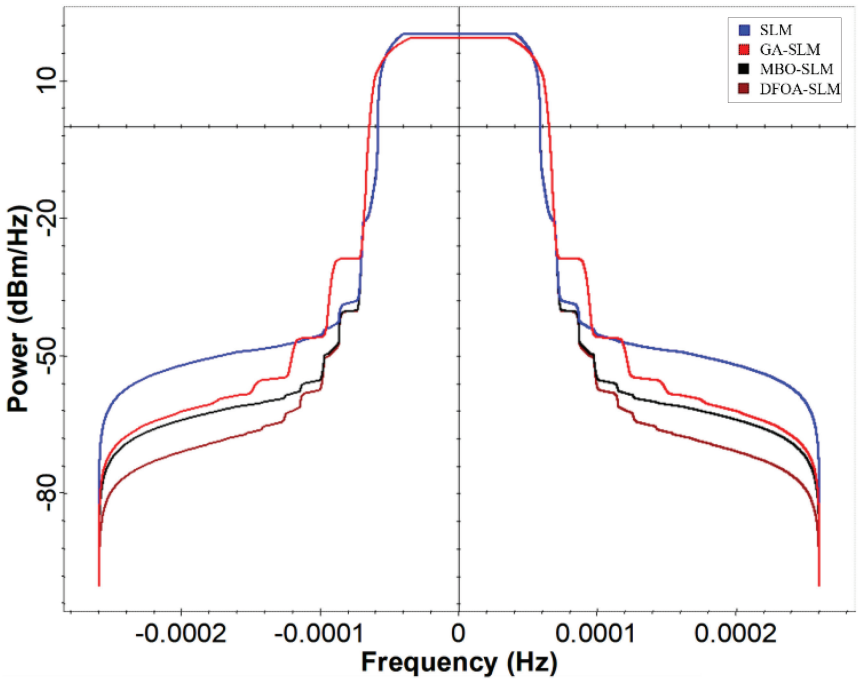

FIGURE 22 | PSD analysis of optical OFDM spectrum after using PAPR reduction methods for the 64-QAM modulation.

Figure 22 shows the PSD performance of the proposed and classical PAPR techniques for 64-QAM on the optical fiber channel. The spectrum leakage values indicated in the graph are approximately −47.5 dBm/Hz for SLM, −48.3 dBm/Hz for GA-SLM, −49.4 dBm/Hz for MBO-SLM, and −53 dBm/Hz for DFOA-SLM, respectively.

Figure 23 shows the PSD performance of the proposed and classical PAPR techniques for 128-QAM on the optical fiber channel. The spectrum leakage values indicated in the graph are approximately −37 dBm/Hz for SLM, −45 dBm/Hz for GA-SLM, −46 dBm/Hz for MBO-SLM, and −52 dBm/Hz for DFOA-SLM, respectively.

Figure 24 shows the PSD performance of the proposed and classical PAPR techniques for 256-QAM on the optical fiber channel. The spectrum leakage values indicated in the graph are approximately −34 dBm/Hz for SLM, −43 dBm/Hz for GA-SLM, −45 dBm/Hz for MBO-SLM, and −51 dBm/Hz for DFOA-SLM, respectively.

It is concluded that the DFOA-SLM demonstrated significant spectral performance within the O-OFDM system. The proposed

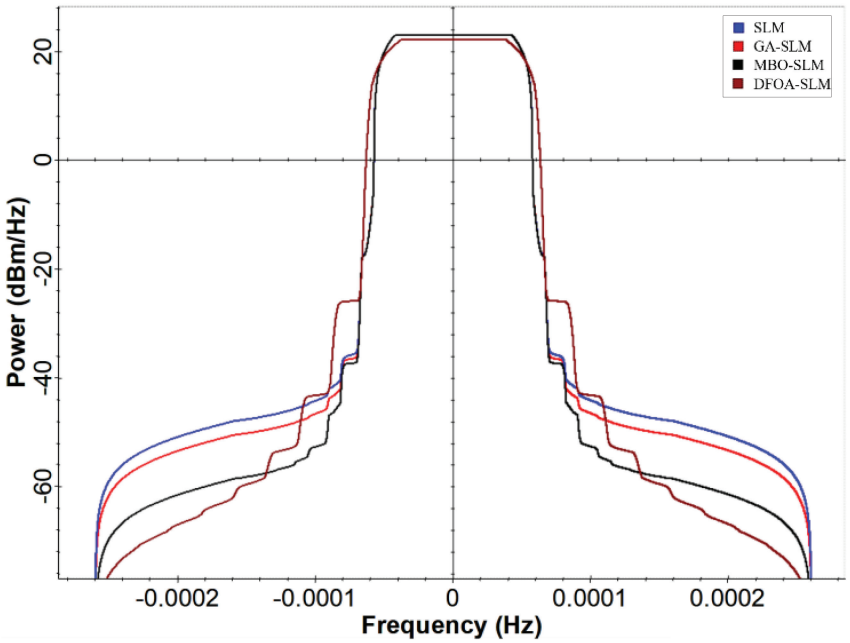

FIGURE 23 | PSD analysis of optical OFDM spectrum after using PAPR reduction methods for the 128-QAM modulation.

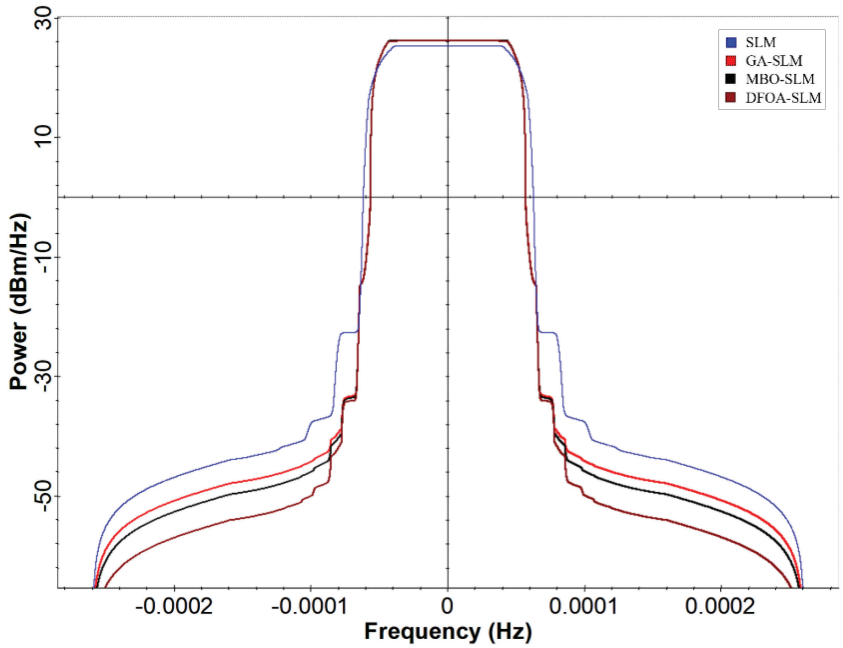

FIGURE 24 | PSD analysis of optical OFDM spectrum after using PAPR reduction methods for the 256-QAM modulation.

PAPR reduction method effectively reduces interference with adjacent channels, improving spectral efficiency. Additionally, lower sidelobes enhance signal integrity and decrease the likelihood of data errors, resulting in better overall performance and reliability in optical communication systems.

Figure 25 illustrates the BER evaluations of the four methods over various OSNR values from 10 to 45 dB for 4-QAM. While the OSNR value will be fixed, the BER of the optical OFDM signal based on SLM method is the maximum; but the BER of the GA-SLM method is less than that of the conventional the SLM method. While the BER equals 10^{-4}, the DFOA-SLM technique needs about 0.98 dB fewer OSNR compared with the MBO-SLM technique, about 1.68 dB fewer OSNR compared with the MBO-SLM technique, and about 2.39 dB fewer OSNR compared with the conventional SLM technique. The DFOA-SLM technique provides better BER performance than other techniques. Table 8 summarizes the OSNR values for each SLM-based techniques at BER as 10^{-4}.

In comparing methods for PAPR reduction, it is essential to consider power-saving performance. This performance is defined by the following:

$$Power\ saving\ (\%) = \frac{Original\ PAPR\ value - Reduced\ PAPR\ value}{Original\ PAPR\ value} \times 100 \quad (15)$$

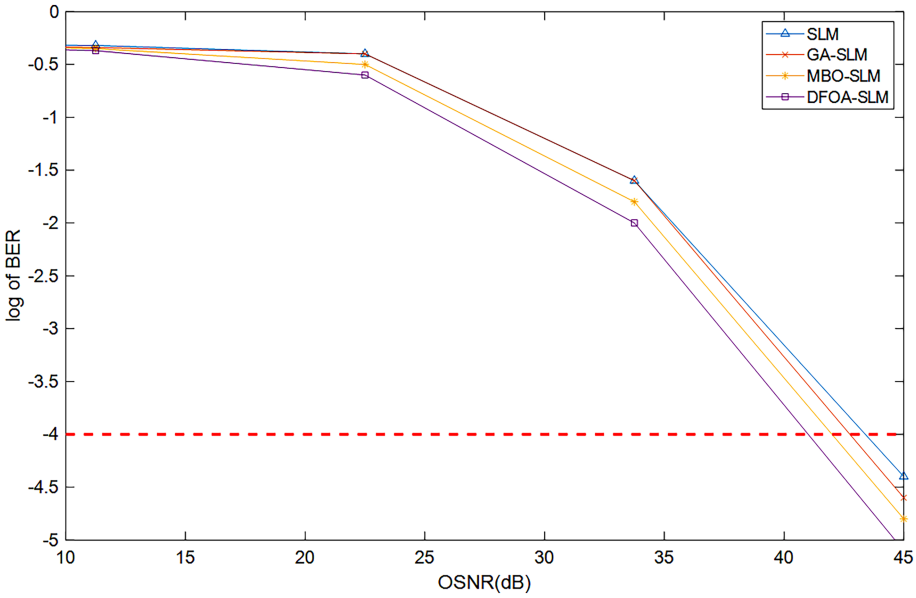

FIGURE 25 | BER performance results for each of the considered SLM-based techniques.

TABLE 8 | OSNR values for each of the considered SLM-based techniques at BER = 10^{-4}.

Technique	OSNR (dB)
SLM (U = 512)	43.46
GA-SLM	42.75
MBO-SLM	42.05
DFOA-SLM	41.07

TABLE 9 | Power saving performance of PAPR reduction methods for 4-QAM.

PAPR reduction method	M-QAM (10.68 dB)
SLM	47.94%
GA-SLM	49.44%
MBO-SLM	53.46%
DFOA-SLM	54.31%

Table 9 summarizes the power saving performance of different PAPR reduction methods on the optical OFDM signal. The proposed DFOA-SLM approach show the best power savings with a maximum of 54.31% for 4-QAM. Other PAPR reduction methods show little power savings with a minimum of 47.94% for the classical SLM method. The results demonstrate that the proposed DFOA-SLM approach provides significant increases in energy efficiency for optical OFDM systems, surpassing other PAPR reduction methods.

7 | Evaluation of the Computational Complexity of the Considered Schemes

The computational complexity of each utilized optimization algorithm was evaluated to show the PAPR minimization performance at a certain CCDF = 10^{-3}. Firstly, the search complexity of the SLM method (Q_{SLM}), denoted as U, is directly proportional to the amount of IFFT processes achieved during the optimal phase sequence search, and it is represented as follows:

$$Q_{SLM} = U.\ N.\ \log_2 N \tag{16}$$

TABLE 10 | Computational complexity of each PAPR reduction method to achieve a 5.56 dB at CCDF = 10^{-3}.

Methods	Computational complexity	Improvement in percentage (%)
SLM	512	0
GA-SLM	352	31.25
MBO-SLM	336	34.37
DFOA-SLM	135	73.63

It is easy to get the computational complexity of modified SLM strategies by taking out the search complexity of SLM given by U from the SLM complexity expression in Equation (16) and replacing it with the search complexity of SLM strategies based on intelligence swarm optimization algorithms. The computational complexities of three optimization methods are evaluated accordingly as below:

$$Q_{DFOA-SLM} = NFC.\ N.\log_2 N \tag{17}$$

$$Q_{MBO-SLM} = ([W + (W - H).(F - 1)].T.\ C).\ N.\ \log_2 N \tag{18}$$

$$Q_{GA-SLM} = P.\ G.\ N.\ \log_2 N \tag{19}$$

The computational complexity of any technique, as outlined in Equations (16)–(19), is primarily influenced by its search complexity. This research standardizes the computational complexities of the assumed methods by setting their

search complexities to a common value of 512. The phase optimization process has enabled intelligent PAPR reduction schemes to achieve a PAPR value of 5.56 dB, surpassing that of the conventional SLM for U equals 512 at a CCDF of 10^{-3}, $SN = G.\ P = 11.\ 32 = 352$ for GA-SLM, $SN = ([W + (W\text{-}H).\ (F\text{-}1)].\ T.\ C) = ([4 + (4 - 1).\ (5 - 1)].\ 4.\ 3) = 336$ for MBO-SLM, and $SN = NFC = 135$ for DFOA-SLM. The computational loads required by GA, MBO, and DFOA based on SLM to achieve similar PAPR results as the classical SLM are evaluated as (315,392), (301,056), and (120,960), respectively. The computational complexity of the SLM method is (458,752) for $SN = 512$, with GA-SLM, MBO-SLM, and DFOA-SLM achieving improvements of 31.25%, 34.37%, and 73.63%, respectively. The proposed DFOA-SLM demonstrates a significant advancement in computational complexity, resulting in a 73.63% reduction in computational load compared with the conventional SLM scheme. The computational complexity of each PAPR reduction method is summarized in Table 10.

8 | Conclusion

This research first analyzed and simulated a low cost-effective IM/DD OFDM communication system with 4 and 16-QAM modulation using MATLAB and OptiSystem software. The constellation diagrams of 4 and 16 QAM, the spectra of the optical signal, and the electrical OFDM signal of the proposed IM/DD OFDM system were analyzed and discussed at a propagation length of 30 km. For PAPR reduction, DFOA-SLM was proposed and applied to the IM/DD optical OFDM system. DFOA-SLM effectively reduced the PAPR of the original optical OFDM signal, achieving significant improvements over the three simulated methods. The proposed PAPR reduction method achieves a PAPR reduction gain of 5.8 dB compared with the original OFDM signal at a CCDF of 10^{-3} while the search number is 512. The proposed PAPR reduction methods show only a slight improvement when the modulation scheme changes from 16 to 4 QAM. For instance, after the modulation scheme changed, the PAPR reductions in DFOA–SLM, MBO–SLM, GA–SLM, and classical SLM techniques at CCDF 10^{-3} are 0.029, 0.0404, 0.012, and 0.007 dB, respectively. The proposed PAPR reduction method improved the transmission power in our IM/DD OFDM system, resulting in an 8 dB improvement. The parameters of the DFOA-SLM algorithm, such as area limit in the forest, lifetime, transfer rate, LSCs, and global seeding changes affect the PAPR performance of our proposed OFDM system. Increasing the area limit parameter from 5 to 25 resulted in a consistent decline in the PAPR reduction performance of the proposed technique. Specifically, when the area limits were set at 5, 15, and 25, the corresponding PAPR values at a CCDF of 10^{-3} were 4.92, 4.96, and 5.04 dB, respectively. When the lifetime parameter was set between 3 and 8, the maximum variation in PAPR at a CCDF of 10^{-3} was only 0.04 dB. In contrast, the best and worst PAPR reduction performances were observed with lifetime parameter values of 1 and 2, respectively. The PAPR values were observed at transfer rates of 5, 15, and 30, with a significant decline in performance at transfer rates higher than 30, with the proposed method showing a PAPR of 5.21 dB at a CCDF of 10^{-3}. The most effective PAPR curve in the first set is achieved with an *LSC* value of 2, and the DFOA-SLM technique yields PAPR values of 5.08, 4.96, and 4.90 dB for the LSC variable values of 1, 2, and 3, respectively. When the *GSC* parameter values are set to 1, 2, 5, and 6, the PAPR values achieved by the proposed method, which is DFOA based on SLM, at a CCDF of 10^{-3} are 4.85, 4.91, 4.95, and 5.01 dB, respectively. The proposed PAPR reduction method enhances spectral efficiency, signal integrity, and reduces data errors, thereby improving overall performance and reliability in optical communication systems. The DFOA-SLM technique offers superior BER performance compared with other techniques, with a lower OSNR of 0.98 dB compared with MBO-SLM, 1.68 dB compared with GA-SLM, and 2.39 dB compared with conventional SLM. Finally, the computational complexity of the DFOA-SLM method shows a 73.63% improvement over the classical SLM method when the search number is set to 512.

Acknowledgments

The authors express their sincere appreciation for the support received from the Smart Grids Laboratory at Istanbul Sabahattin Zaim University, particularly for their invaluable assistance with software support. This research was additionally funded by the Erciyes University Scientific Research Projects Coordination Unit (Project No. FDK-2019-8750).

Conflicts of Interest

The authors declare no conflicts of interest.

Data Availability Statement

No data was used for the research described in the article.

References

1. H. Rohling, *OFDM Concepts for Future Communication Systems* (Springer, 2011), https://doi.org/10.1007/978-3-642-17496-4.

2. A. Sharif, "PAPR Reduction of Optical OFDM Signals in Visible Light Communications," *ICT Express* 5 (2019): 202–205, https://doi.org/10.1016/j.icte.2019.01.001.

3. K. Mhatre, "Efficient Selective Mapping PAPR Reduction Technique," *Procedia Computer Science* 45 (2015): 620–627, https://doi.org/10.1016/j.procs.2015.03.117.

4. I. Ahmed, H. Karvonen, T. Kumpuniemi, and M. Katz, "Wireless Communications for the Hospital of the Future: Requirements, Challenges, and Solutions," *International Journal of Wireless Information Networks* 27 (2020): 4–17, https://doi.org/10.1007/s10776-019-00468-1.

5. A. Chaaban, Z. Rezki, and M. Alouini, "On the Capacity of Intensity-Modulation Direct-Detection Gaussian Optical Wireless Communication Channels," *IEEE Communications Surveys & Tutorials* 24 (2022): 455–491, https://doi.org/10.1109/COMST.2021.3120087.

6. S. Hameed, A. Sabri, and S. Abdulsatar, "A Novel PAPR Reduction Method for ADO-OFDM VLC Systems," *Optical and Quantum Electronics* 53, no. 10 (2021): 595, https://doi.org/10.1007/s11082-021-03251-w.

7. N. Taşpınar and M. Alhalabi, "Performance Investigation of Long-Haul High Data Rate Optical OFDM IM/DD System With Different QAM Modulations," *Journal of Electrical Engineering-Elektrotechnicky Casopis* 72 (2021): 192–197, https://doi.org/10.2478/jee-2021-0026.

8. L. Chen, B. Krongold, and J. Evans, "Performance Analysis for Optical OFDM Transmission in Short-Range IM/DD Systems," *Journal of Lightwave Technology* 30 (2012): 974–983, https://doi.org/10.1109/JLT.2012.2185779.

9. S. Singhal and D. Sharma, "A Review and Comparative Analysis of PAPR Reduction Techniques of OFDM Systems," *Wireless Personal*

Communications 135 (2024): 777–803, https://doi.org/10.1007/s11277-024-11074-7.

10. S. Mondal, "Approach to Reduce PAPR in Orthogonal Frequency Division Multiplexing Technique," *Turkish Journal of Computer And Mathematics Education* 12 (2021): 4480–4484, https://turcomat.org/index.php/turkbilmat/article/view/5186.

11. B. Noursabbaghi, G. Baghersalimi, A. Pouralizadeh, and O. Mohammadian, "PAPR Reduction in OFDM UOWC System Employing Repetitive Clipping and Filtering (RCF) Method," *Journal of Electrical and Computer Engineering Innovations* 11 (2023): 301–310, https://doi.org/10.22061/jecei.2022.9061.569.

12. M. Rana, T. Tithy, N. Rahman, and M. Hasan, "PAPR Reduction Techniques and Their Bit Error Rate Measurement at OFDM in LTE System," *International Journal on AdHoc Networking Systems (IJANS)* 12 (2022).

13. B. Faraj and A. Siddiq, "Peak to Average Power Ratio Reduction for OFDM With IM System," in *2022 4th International Conference on Advanced Science and Engineering (ICOASE)* (IEEE, 2022), 95–100, https://doi.org/10.1109/ICOASE56293.2022.10075595.

14. A. Abdulhussein and N. Hikmat, "Comparative Study of Peak to Average Power Ratio in OFDM and FBMC Systems," in *2021 7th International Conference on Space Science and Communication (IconSpace)* (IEEE, 2021), 140–145, https://doi.org/10.1109/IconSpace53224.2021.9768772.

15. S. Krikunov, R. Bychkov, A. Blagodarnyi, and A. Ivanov, "Clustering and Fitting to Reduce PAPR in Multi-User OFDM Systems," in *25th International Conference on Digital Signal Processing and It's Applications (DSPA)* (IEEE, 2023), 1–6, https://doi.org/10.1109/DSPA57594.2023.10113449.

16. N. Taşpınar and M. Alhalabi, "Peak-to-Average Power Ratio (PAPR) Reduction Using Discrete Invasive Weed Optimization (DIWO) in Coherent Detection Optical OFDM (CO-OFDM) Communication Systems," *Wireless Personal Communications* 139 (2024): 715–732, https://doi.org/10.1007/s11277-024-11645-8.

17. S. Prasad and S. Arun, "Hanowa Matrix Based SLM Technique for PAPR Reduction in OFDM Systems," in *2023 International Conference for Advancement in Technology (ICONAT)* (ICONAT, 2023), 1–5, https://doi.org/10.1109/ICONAT57137.2023.10080797.

18. P. Priyanka, R. Shaik, K. Vijaya, P. Sasi, P. Ruthvik, and A. Raja, "Improved MFO Algorithm Based PTS Scheme in OFDM Systems for PAPR Reduction," in *4th International Conference on Signal Processing and Communication (ICSPC)* (IEEE, 2023), 153–157, https://doi.org/10.1109/ICSPC57692.2023.10125973.

19. I. Ishmiev and S. Loginov, "M-Sequence Based Partial Transmit Sequence PAPR Reduction Technique," in *Systems of Signals Generating and Processing in the Field of on Board Communications* (IEEE, 2023), 1–5, https://doi.org/10.1109/IEEECONF56737.2023.10092029.

20. Y. Tu and C. Chang, "A Novel Low Complexity Two-Stage Tone Reservation Scheme for PAPR Reduction in OFDM Systems," *Sensors* 23 (2023): 950, https://doi.org/10.3390/s23020950.

21. Y. Yuan, S. Wei, X. Luo, Z. Xu, and X. Guan, "Adaptive PTS Scheme Based on Fuzzy Neural Network for PAPR Reduction in OFDM System," *Digital Signal Processing* 126 (2022): 103492, https://doi.org/10.1016/j.dsp.2022.103492.

22. V. Padarti, C. Dasari, P. Dokala, V. Chowtapalli, and L. Avula, "An Efficient Clipping Method for PAPR Reduction in OFDM Systems," in *International Conference on Inventive Computation Technologies* (IEEE, 2022), 624–629, https://doi.org/10.1109/ICICT54344.2022.9850836.

23. N. Sivadas, "PAPR Reduction of OFDM Systems Using H-SLM Method With a Multiplierless IFFT/FFT Technique," *ETRI Journal* 44 (2022): 379–388, https://doi.org/10.4218/etrij.2020-0316.

24. S. Prasad, S. Arun, and S. Chandana, "Selective Mapping Technique With Novel Symmetric Hankel Phase Sequences for PAPR Reduction in OFDM Systems," *International Journal of Mechanical Engineering* 7 (2022): 1047–1058.

25. Z. Ibraheem, K. Ahmed, Y. Fazea, and M. Madi, "Boosted PTS Method With Mu-Law Companding Techniques for PAPR Reduction in OFDM Systems," *Wireless Personal Communications* 124 (2022): 423–436, https://doi.org/10.1007/s11277-021-09366-3.

26. A. Mayakannan, C. Arvind, P. Dhinakar, et al., "Neural Network-Based Regression Assisted PAPR Reduction Method for OFDM Systems," *Sādhanā* 47, no. 4 (2022): 242, https://doi.org/10.1007/s12046-022-02024-9.

27. J. Yu, J. Liu, Y. Ma, and Z. Liu, "PAPR Reduction in OFDM System Using a New Quantum Genetic Algorithm," in *2021 5th International Conference on Electronic Information Technology and Computer Engineering* (2021), 1056–1060, https://doi.org/10.1145/3501409.3501597.

28. F. Zou, Z. Liu, H. Xin, and G. Wang, "A Novel PAPR Reduction Scheme for OFDM Systems Based on Neural Networks," *Wireless Communications and Mobile Computing* 2021 (2021): 5574807, https://doi.org/10.1155/2021/5574807.

29. Z. Xing, K. Liu, A. Rajasekaran, H. Yanikomeroglu, and Y. Liu, "A Hybrid Companding and Clipping Scheme for PAPR Reduction in OFDM Systems," *IEEE Access* 9 (2021): 61565–61576, https://doi.org/10.1109/ACCESS.2021.3074009.

30. A. Kumar, K. A. P. Yaminiand, K. Kaliaperumal, R. A. Alsowail, and G. Nishant, "A Systematic PAPR Analysis of Optical 5G Waveforms Using Advanced and Deep Learning PAPR Algorithms: Estimation of PAPR, PSD, and BER," *Wireless Networks* 31 (2025): 1861–1883, https://doi.org/10.1007/s11276-024-03835-w.

31. A. Kumar, R. Sarveswara, G. Babu, N. Gaur, and A. Nanthaamornphong, "Analysis of PAPR Reduction Algorithms for Optical OFDM 5G Radio Waveform System for Visible Light Communication," *Journal of Optical Communications* (2025), https://doi.org/10.1515/joc-2024-0276.

32. M. Wu, J. Zhang, Y. Xie, Y. Shi, and T. Yao, "Peak-to-Average Power Ratio Reduction Scheme in DCO-OFDM With a Combined Index Modulation and Convex Optimization," *IEICE Transactions on Fundamentals of Electronics, Communications and Computer Sciences* 107–A (2024): 1425–1429, https://doi.org/10.1587/transfun.2023EAL2113.

33. Y. Zenhom, K. I. Hamad, M. Alghassab, and M. M. Elnabawy, "Optical-OFDM VLC System: Peak-to-Average Power Ratio Enhancement and Performance Evaluation," *Sensors* 24, no. 10 (2024): 2965, https://doi.org/10.3390/s24102965.

34. R. Bauml, R. Fischer, and J. Huber, "Reducing the Peak-to-Average Power Ratio of Multicarrier Modulation by Selected Mapping," *Electronics Letters* 32 (1996): 2056–2057, https://doi.org/10.1049/el:19961384.

35. C. Wang and Y. Quyang, "Low-Complexity Selected Mapping Schemes for Peak-to-Average Power Ratio Reduction in OFDM Systems," *IEEE Transactions on Signal Processing* 53 (2005): 4652–4660, https://doi.org/10.1109/TSP.2005.859327.

36. N. Taşpınar and Ş. Şimşir, "Advanced SLM Scheme Based on Discrete Forest Optimization Algorithm for PAPR Minimization in UFMC Waveform," *Wireless Networks* 27 (2021): 1353–1368, https://doi.org/10.1007/s11276-020-02515-9.

37. A. Kabli and M. Faqihi, "Optical OFDM (O-OFDM) for Intensity Modulated/Direct Detection Optical Systems, Networks and Satellite," in *Comnetsat 2018—Proceedings* (2019), 34–38, https://doi.org/10.1109/COMNETSAT.2018.8684118.

38. K. Tahkoubit, H. Shaiek, D. Roviras, S. Faci, and A. Ali-Pacha, "Generalized Iterative Dichotomy PAPR Reduction Method for Multicarrier Waveforms," *IEEE Access* 9 (2021): 114235–114245, https://doi.org/10.1109/ACCESS.2021.3102848.

39. A. Abdulkafi, M. Alias, Y. Hussein, and N. Omar, "PAPR Reduction of DC Biased Optical OFDM Using Combined Clipping and PTS Techniques," in *2017 IEEE 13th Malaysia International Conference on Communications (MICC), The Puteri Pacific, Johor Bahru, Malaysia* (2017), https://doi.org/10.1109/MICC.2017.8311760.

40. H. Freag, E. Hassan, S. El-Dolil, and M. Dessouky, "New Hybrid PAPR Reduction Techniques for OFDM-Based Visible Light Communication Systems," *Journal of Optical Communications* 39 (2018): 427–435, https://doi.org/10.1515/joc-2017-0002.

41. M. Ghaemi and M. Derakhshi, "Forest Optimization Algorithm," *Expert Systems with Applications* 41 (2014): 6676–6687, https://doi.org/10.1016/j.eswa.2014.05.009.

42. M. Ghaemi and M. Derakhshi, "Feature Selection Using Forest Optimization Algorithm," *Pattern Recognition* 60 (2016): 121–129, https://doi.org/10.1016/j.patcog.2016.05.012.